

**Popular Democratic Republic of Algeria**  
Ministry of Higher Education and Scientific Research  
Ibn Khaldoun University – Tiaret  
Sciences Applique Faculty  
Department of Mechanical Engineering



**Dissertation submitted in partial fulfillment of the requirements for the  
Master's Degree in the Field of Mechanical Engineering**

**Domain:** Sciences and Technology

**Field:** Mechanical Engineering

**Major:**

**Numerical study of the dynamic behavior of a  
hydrostatic bearing with four pads lubricated  
by a micropolar fluid**

**Submitted by:**

BOUHENNI Abdelhamid

**Supervised by:**

Mr. BENARIBA Aboubakeur

**Publicly defended on:** 22/06/2024

**Board of Examiners**

<b>Names</b>	<b>Grade</b>	<b>University of Reattachment</b>	<b>Quality</b>
DEBBIH Senouci	MAA	University of Tiaret	President
MAKHFI Souad	MCA	University of Tiaret	Examiner
HAMMOU Mahmoud	MCB	University of Tiaret	Examiner
BENARIBA Aboubakeur	MCA	University of Tiaret	Supervisor
ABOUSHIGHIBA Hicham	MCB	University of Tiaret	Supervisor

**Academic Year: 2023/2024**

بِسْمِ الرَّحْمَنِ الرَّحِيمِ

***Dedication***

*In loving memory of my grandma,  
To my dear mom and my whole family.  
To all those who are dear to me.  
To all my friends.  
I dedicate this work*

BOUHENNI Abdelhamid

## ***Acknowledgements***

*First and foremost, I thank Almighty God who gave me the will and courage to complete this modest work.*

*I warmly thank my supervisor, **Mr. BENARIBA Aboubakeur**, for his availability, his attention to my work, his wise advice, and his encouragements, which have been of great importance in the development and successful completion of this research.*

*I wish to extend my heartfelt thanks to **Mr. ABOUSHIGHIBA Hicham** for the priceless advice he has provided over the past two years. His guidance has significantly impacted our education.*

*I sincerely thank **Mr. DEBBIH** for the great honor of having accepted to chair the defense jury.*

*I also thank the jury members, **Mr. HAMMOU** and **Mrs. MAKHFI** for honoring us by agreeing to judge our work.*

*Finally, i thank all those who have contributed, directly or indirectly, to the realization of this work.*

### ملخص

يقدم هذا العمل دراسة رقمية حول تأثيرات الخصائص المميزة لسائل الميكروبولار و نسبة الضغط على محور هيدروستاتيكي بأربع وسائد هيدروستاتيكية يغذيها السائل عن طريق قناة شعيرية. لتحديد توزيع الضغط، يتم حل معادلة رينولدز المعدلة باستخدام طريقة الفروق المحدودة و طريقة غوس سيدال. تظهر النتائج أن المحامل التي تعمل بزيوت التشحيم ميكروبولار تظهر زيادة في الضغط في الخلية، مما يشير إلى أن الأداء يتأثر بشكل رئيسي بنسبة الضغط

### الكلمات الدلالية

سائل الميكروبولار، حامل هيدروستاتيكي، معادلة رينولدز المعدلة، طريقة الفروق المحدودة

### Abstract

This work presents a numerical study on the effects of characteristic parameters of micropolar fluids and the pressure ratio on a four-pad hydrostatic bearing used as a hydrostatic squeeze film through capillary-type hydraulic resistances. To determine the pressure distribution, the modified Reynolds equation is solved using the finite difference method and the Gauss-Seidel iteration. The results show that bearings lubricated by micropolar fluids exhibit an increase in pressure in the recesses, suggesting that performance is mainly influenced by the pressure ratio.

**Key words:** Micropolar lubricant, hydrostatic bearing, modified Reynolds equation, finite difference method.

### Résumé

Ce travail présente une étude numérique sur les effets des paramètres caractéristiques des fluides micropolaires et du rapport de pression sur un palier hydrostatique à quatre patins utilisé comme *'hydrostatic squeeze film damper'* à travers des résistances hydrauliques de type capillaire. Pour déterminer la distribution de pression, l'équation de Reynolds modifiée est résolue en utilisant la méthode des différences finies et l'itération de Gauss-Seidel. Les résultats montrent que les paliers lubrifiés par des fluides micropolaires présentent une augmentation de la pression dans les alvéoles, suggérant que les performances sont principalement influencées par le rapport de pression.

**Mots clés:** Lubrifiant micropolaire, palier hydrostatique, l'équation de Reynolds modifiée, méthode des différences finies.

---

## Content

Dedication	II
Acknowledgements	III
Abstract	IV
Contents	V
List of figures	VI
List of tables	VI
Appendix	VII
General Introduction	1
<b>Chapter I bibliographic study</b>	
I.1 Introduction	4
I.2 The bearings	4
I.2.1 Roller bearings	4
I.2.1.1 Advantages of roller bearings	5
I.2.1.2 Disadvantages of roller bearings	5
I.2.2 Magnetic bearings	5
I.2.2.1 Advantages of magnetic bearings	6
I.2.2.2 Disadvantages of magnetic bearings	6
I.2.3 Hydrodynamic bearings	6
I.2.3.1 Operating principle	7
I.2.4 Hydrostatic Bearing	8
I.2.4.1 Classification of Hydrostatic Bearings	8
I.2.4.1.1 Thrust Bearings	9
I.2.4.1.2 Multi-directional Pads	10
I.2.4.1.3 Radial Pads	11
I.2.4.2 hydrostatic bearings with three pads	11

---

I.2.4.3 Hydrostatic Four-Pad Bearing	12
I.2.4.4 The advantages and disadvantages of hydrostatic bearings	12
I.2.4.5 Geometric characteristics of hydrostatic bearings	13
I.2.5 Hydrostatic lubrication	14
I.2.5.1 Definition	14
I.2.5.2 Principle of hydrostatic lubrication	15
I.2.5.3 Formation of the hydrostatic fluid film	17
I.2.5.4 Hydraulic Resistances	18
I.3 Lubricants	20
I.3.1 Newtonian Fluid	20
I.3.2 Non-Newtonian Fluid	20
I.3.3 Complex Fluid	20
I.3.4 Micropolar Fluids	21
I.3.5 Micropolar Lubrication	22
I.3.5.1 Definition	22
I.3.5.2 Some application of micropolar lubrication	22
I.3.5.3 Equations of Micropolar Lubrication	23
I.3.5.4 Hypothesis and Demonstration	25
I.4 The dynamics of the rotors	28
I.4.1 Predictions of the dynamic behavior of rotors	29
I.4.2 Objectives of the dynamic analysis of rotors	29
I.5 Conclusion	30
<b>Chapter II Hydrostatic Bearing with four pads Lubricated by a Micropolar Fluid.</b>	
II.1 Introduction	31
II.2 Study of a hydrostatic squeeze film damper	31
II.2.1 The modified Reynolds equation	34
II.2.1.1 Discretization of the Modified Reynolds Equation	35

---

II.2.1.2 Numerical Solution of the System of Equations	37
II.2.2 Performance characteristics	39
II.2.2.1 Load-carrying capacity	39
II.2.2.2 Recess pressure	39
II.2.2.3 Total lubricant flow rate	41
II.2.2.4 Dynamic characteristics	41
II.2.2.5 Equivalent Dynamic Coefficients	44
II.3 Validation of the Numerical Model	44
II.4 Conclusion	45
<b>Chapter III Results and discussion</b>	
III.1 Introduction	47
III.2 Solution procedure	47
III.3 Results and discussion	47
III.4 Validation of numerical model	48
III.5 Study of the influence of micropolar fluid parameters	51
III.5.1 Influence of micropolar fluid parameters on pressure profile	51
III.5.2 Influence of micropolar fluid parameters on equivalent stiffness	51
III.5.3 Influence on equivalent damping	53
III.5.4 Influence on damping factor	54
III. Conclusion	55
General Conclusion	57
References	59

**Liste of figures**

Figure I.1	Rollar bearings	5
Figure I.2	Magnetic bearings	6
Figure I.3	Hydrodynamic bearings	7
Figure I.4	Phases of the hydrodynamic regime	8
Figure I.5	Hydrostatic bearing	9
Figure I.6	Circular Pad	10
Figure I.7	Rectangular Pads	10
Figure I.8	Conical Pads	11
Figure I.9	Multi-directional Pads	11
Figure I.10	Radial Pads	12
Figure I.11	Schematic representation of a three-pad hydrostatic bearing	12
Figure I.12	Schematic representation of a four-pad hydrostatic bearing	13
Figure I.13	Rheological behavior of time-dependent fluids	15
Figure I.14	Schematization of a hydrostatic thrust bearing	15
Figure I.15	Constant pressure supply	16
Figure I.16	Constant flow supply	17
Figure I.17	Formation of the fluid film in a hydrostatic thrust bearing	17
Figure I.18	Schematic diagram of a damping film bearing (SFD)	18
Figure I.19	Capillary-Type Hydraulic Resistance	19
Figure I.20	Hydraulic resistance of orifice type	19
Figure I.21	Geometry and Kinematics of Contact	26
Figure I.22	An example of a rotor	29
Figure II.1	Hydrostatic squeeze film damper geometry	32
Figure II.2	Diagram of a single-acting hydrostatic thrust bearing	33
Figure II.3	Boundary conditions of a hydrostatic thrust bearing	34

Figure II.4	Calculation domain	35
Figure II.5	Description of a node	36
Figure II.6	Discretization of one-quarter of the integration domain	37
Figure II.7	Flow rate exiting the recess	40
Figure II.8	Stiffness and damping of the $i$ th hydrostatic bearing pad	42
Figure II.9	Pad of the infinitely long hydrostatic thrust bearing	45
Figure III.1	Comparison of the numerical and analytical results	50
Figure III.2	Pressure distribution for various values of $N_2$ with $L_m=5$	51
Figure III.3	Variation of equivalent stiffness as a function of eccentricity ratio	52
Figure III.4	Variation of equivalent stiffness as a function of $L_m$	52
Figure III.5	Variation of equivalent damping as a function of eccentricity ratio	53
Figure III.6	Variation of equivalent damping as a function of $L_m$	54
Figure III.7	Variation of damping factor as a function of eccentricity ratio	54
Figure III.8	Variation of damping factor as a function of $L_m$	55

## Liste of tables

Table III.1	Simulation parameters.	48
-------------	------------------------	----

## Appendix

$a$	recess length [m]
$A$	bearing pad length [m]
$b$	Recess width [m]
$B$	Bearing pad width [m]
$C_{pi}$	damping coefficient relative to each pad [N.s/m]
$C_{eq}$	equivalent damping coefficient [N.s/m]
$dc$	diameter of the capillary [m]
$e_x, e_y$	eccentricities along x and y respectively [m]
$h_0$	film thickness at the center position of the hydrostatic squeeze film dampers [m]
$h_i$	film thickness of the $i^{\text{th}}$ hydrostatic bearing pad [m]
$\dot{h}_i$	the squeeze velocity of the movable grain relative to the single-acting thrust bearing
$I_0$	modifier Bessel functions of zeroth and first kind
$I_1$	modifier Bessel functions of first order and first kind
$K_{pi}$	stiffness coefficient relative to each pad [N/m]
$K_{eq}$	equivalent stiffness coefficient [N/m]
$lc$	length of the capillary [m]
$l_m$	Length of the micropolar particle
$N$	The coupling number
$P_{ri}$	recess pressure of the $i^{\text{th}}$ hydrostatic bearing pad [Pa]
$P_{ro}$	recess pressure at the center position of the hydrostatic squeeze film dampers [Pa]
$Q_{vi}$	Outgoing flow from the recess in the x and z directions respectively for each pad [ $\text{m}^3/\text{s}$ ]
$Q_{ri}$	Flow through the capillary relative to each pad [ $\text{m}^3/\text{s}$ ]
$Q_{xi}, Q_{zi}$	The flow due to the volume variation in the recess relative to each pad [ $\text{m}^3/\text{s}$ ]
$Q_T$	Total lubricant flow rate [ $\text{m}^3/\text{s}$ ]

$S_r$	surface area of the recess [m <sup>2</sup> ]
$R$	capillary radius [m]
$u_{xi}$	velocity in the x direction of the i <sup>th</sup> hydrostatic bearing pad [m/s]
$u_{zi}$	velocity in the z direction of the i <sup>th</sup> hydrostatic bearing pad [m/s]
$u_r$	velocity in the micropolar flow [m/s]
$W_{pi}$	load-carrying capacity relative to each pad [N]
$(x_i, y_i, z_i)$	coordinate system used in the Reynolds equation
$\beta_0 = P_{r0} / P_s$	ratio of recess pressure over supply pressure at the center position of hydrostatic squeeze film dampers
$\varepsilon = e / h_0$	eccentricity ratio
$\mu$	the viscosity coefficient of the Newtonian fluid [Pa.s]
$\mu_v$	the effective viscosity coefficient of the micropolar fluid [Pa.s]
$\zeta$	damping factor

# **General Introduction**

### General Introduction

In the field of mechanical engineering, the design and optimization of hydrostatic bearings play an essential role in the performance and durability of rotating machinery. These components, used to support and guide rotating shafts, require particular attention regarding their dynamic behavior to ensure reliable and efficient operation of the mechanical systems in which they are integrated.

In this perspective, the numerical study of the dynamic behavior of hydrostatic bearings holds paramount importance for engineers and researchers in the field. With the advent of sophisticated computational tools, it has become possible to delve deeper into the fluid-structure interactions and predict the performance of these bearings under diverse conditions.

This study specifically focuses on the numerical analysis of a particular type of hydrostatic bearing, namely the four-pad bearing lubricated by a micropolar fluid. This study is structured into three chapters, each addressing a critical aspect of this study. The first chapter provides an overview of the fundamentals, ranging from the classification of bearings to rotor dynamics, through hydrostatic lubrication and the specifics of micropolar fluids.

The second chapter delves into the mathematical modeling of hydrostatic bearings with four pads lubricated by micropolar fluids. This chapter details the development of the mathematical models and the assumptions made to simulate the complex interactions within the bearing system. The modeling approach forms the backbone of our numerical analysis and sets the stage for the investigations presented in the following chapter.

The third chapter presents the results and discussion of the numerical analysis, focusing on the influence of micropolar fluid parameters on key performance metrics of a four-pad hydrostatic bearing. These metrics include pressure distribution, stiffness coefficient, damping coefficient, damping factor, load-carrying capacity, and fluid flow. Through detailed analysis, we explore how different parameters of the micropolar fluid impact these critical aspects, providing insights that could lead to significant improvements in bearing design and performance.

In summary, this thesis aims to enhance the understanding of hydrostatic bearings lubricated by micropolar fluids through comprehensive numerical analysis. The findings are expected to contribute to the advancement of design and optimization techniques for mechanical systems, offering new perspectives for innovation in lubrication and tribology.

**Chapter I:**  
**Bibliographic study**

### **I.1 Introduction:**

In this first chapter, we begin our exploration of the dynamic behavior of four-pad hydrostatic bearings lubricated by a micropolar fluid. To do so, we start with an overview of the fundamentals, ranging from the classification of bearings to rotor dynamics, through hydrostatic lubrication and the specifics of micropolar fluids. Bearings, essential in mechanical systems, will first be classified according to their operating characteristics. We will then delve into hydrostatic lubrication, which relies on the use of pressurized fluids to reduce friction and protect moving surfaces. Special attention will be given to micropolar fluids, characterized by unique rheological properties, thus offering interesting prospects for improving the tribological performance of hydrostatic bearings. Finally, we will examine rotor dynamics, a crucial aspect to ensure the proper functioning of rotating machinery interacting with hydrostatic bearings.

### **I.2 The bearings:**

The Bearings are fixed mechanical components designed to support shafts. The role of bearings is to guide and support the transmission shafts of a machine (thermal engines, compressors...), allowing relative movement between two surfaces through the use of lubricants and guiding materials adapted to the issue, known as anti-friction materials. This movement is slowed down by a resisting force which has the effect of: causing wear, consuming energy, and generating heat. The most commonly used types of bearings are rolling bearings, magnetic, hydrodynamic, and hydrostatic bearings [1].

#### **I.2.1 Roller bearings:**

In a roller bearing, the sliding of the shaft on the bearing is replaced by the rolling of intermediate bodies (balls, rollers, and needles). They support higher loads while reducing wear and friction due to their very low friction coefficient at startup. Roller bearings are part of mass-produced components used to support axles, shafts, and moving parts of machines in rotational or translational motion [1].



Figure I.1: Rollar bearings [30].

### **I.2.1.1 Advantages of roller bearings:**

- Simple and easy installation, easy to replace
- Longer lifespan
- Possibility of lifetime lubrication
- Ability to support combined loads
- Low cost and no friction phenomenon
- Better tolerance to temporary lubrication interruptions
- Provide better radial and axial alignment and exhibit low starting torque even at low temperatures

### **I.2.1.2 Disadvantages of roller bearings:**

- Greater fatigue issues
- Low damping capacity
- Significant radial size
- Noise generation
- Limited rotational frequency
- Limited nominal diameter

### **I.2.2 Magnetic bearings:**

Magnetic bearings are used when other bearings have reached their limit. They allow a rotor to rotate without friction or contact. They mainly consist of electromagnets that create a supporting magnetic field. Position sensors control the intensity of the field to keep the shaft at

the center of the bearing. Their preferred domain concerns applications with very high rotational speeds. These bearings have very high precision guidance [2].



Figure I.2: Magnetic bearings [27].

### I.2.2.1 Advantages of magnetic bearings:

- Magnetic bearings are contactless and can be used in vacuum techniques, clean and sterile chambers, and for transporting aggressive or pure fluid media.
- Highest speeds are possible, even up to the rotor's breaking strength.

### I.2.2.2 Disadvantages of magnetic bearings:

- Absence of lubrication seals allows for a larger and stiffer rotor shaft.
- Absence of mechanical wear results in lower maintenance costs and longer system lifespan.
- Adaptable stiffness can be used in vibration isolation, passing critical speeds, and robust against external disturbances.

### I.2.3 Hydrodynamic bearings:

These are known as fluid film bearings, specifically hydrodynamic bearings and thrust bearings in which a thin film of fluid separates the contacting and relatively moving surfaces. This type of bearings is commonly used to support radial loads for guiding large-sized rotors. They are designed to operate under harsh conditions (high loads and rotational frequencies) [3].



Figure I.3: Hydrodynamic bearings [25] [26].

### I.2.3.1 Operating principle:

The operation of the bearing relies on the flow of the film. The adhesion of the thin film lubricant to the moving surfaces generates the flow. In the case of hydrodynamic lubrication, pressure is generated by the conservation of flow in the lift and friction. In the case of a hydrodynamic bearing, the desired lift and friction are consequences. For the liquid to be an effective interface, it is necessary for the pressure field to balance the normal load depending on the available contact surface, while ensuring that the minimum film thickness exceeds any geometric defects in the surfaces [4].

Figure I.4 illustrates the three phases observed during the startup of a loaded bearing.

**Phase (a):** At rest (Figure I.4.a), the shaft and the bearing are in contact, the common generatrix opposes the load, and the distance  $O_a O_c$  is equal to the radial clearance  $C$ .

**Phase (b):** During startup (Figure I.4.b), the shaft slides within the bearing, the lubrication regime is mixed, and the lubricant is drawn into the converging space formed by the shaft and the bearing.

**Phase (c):** Once the rotational speed becomes sufficient (Figure I.4.c), there is the presence of a hydrodynamic pressure field that supports the constant load  $P$ . The center of the shaft  $O_a$  occupies a fixed position within the bearing. If the external force system reduces to a single force  $P$  acting in the planes of the bearing's midsection, the shaft and bearing axes are parallel.

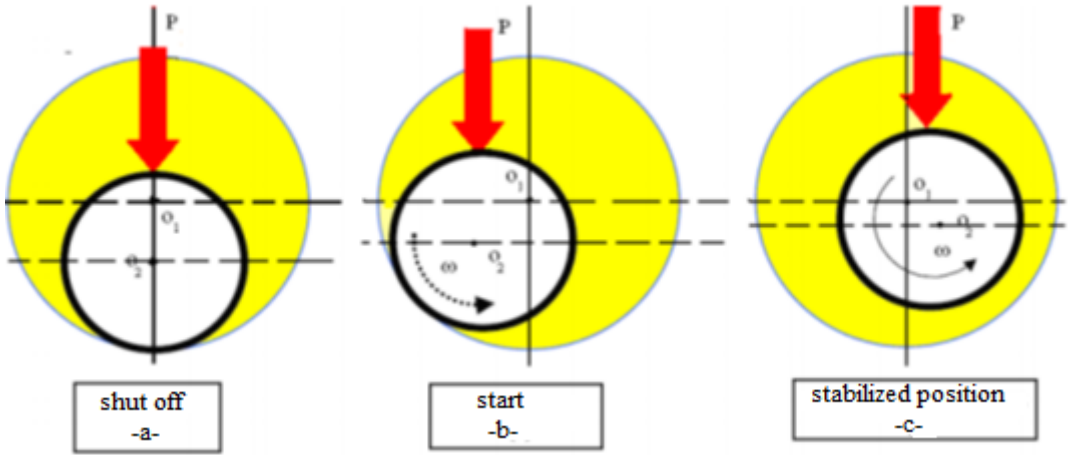


Figure I.4: Phases of the hydrodynamic regime [4].

**I.2.4 Hydrostatic Bearing:**

In a hydrostatic bearing, the separation of surfaces is achieved by a pressurized fluid introduced by an external system, allowing it to support a load and eliminate any metal-to-metal contact. They are successfully used in a wide range of machines operating at low speeds and supporting heavy loads. However, the use of a hydrostatic bearing in high-speed machines as a "spring-damper" support compared to other types of bearings is not common. The hydrostatic bearing offers better stability due to its high rigidity and good damping even when crossing critical speeds. These bearings are employed when the kinematic conditions are not sufficient or stable to achieve hydrodynamic lift (frequent startups, shaft oscillations) [5].



Figure I.5: Hydrostatic bearing [28].

**I.2.4.1 Classification of Hydrostatic Bearings:**

Hydrostatic bearings can be classified based on the direction of the load they can carry. Thus, we have:

- Thrust Bearings.
- Radial Bearings (plain bearings).
- Multi-directional Bearings.

### I.2.4.1.1 Thrust Bearings:

These bearings are mainly composed of three types of pads:

- Opposed Circular Pad.
- Rectangular Pads.
- Conical Pads.

#### ➤ Circular Opposed Pads:

Figure I.6 depicts the schematic of a circular pad [6]. When the load can act in two directions, or when greater rigidity is required, two circular pads can be assembled.

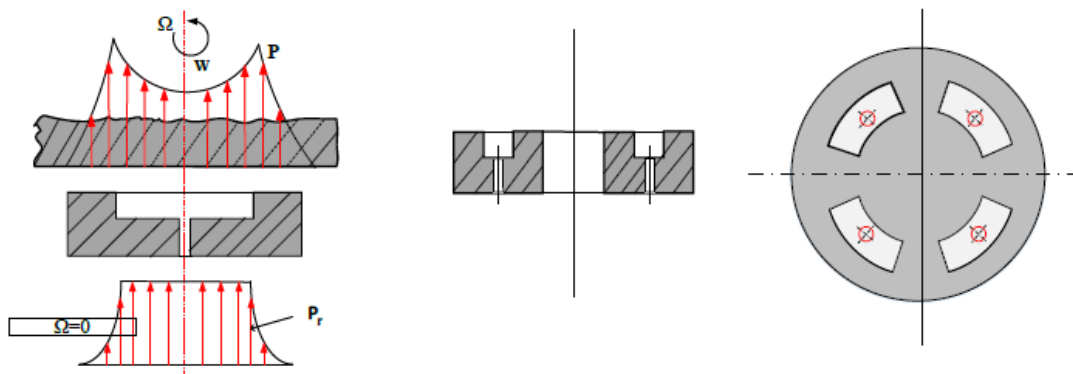


Figure I.6: Circular Pad [6].

#### ➤ Rectangular Pads

Figure I.7 shows several shapes of rectangular pads. In order to have a hybrid behavior, the pads should move at very high speed and have a fixed inclination.

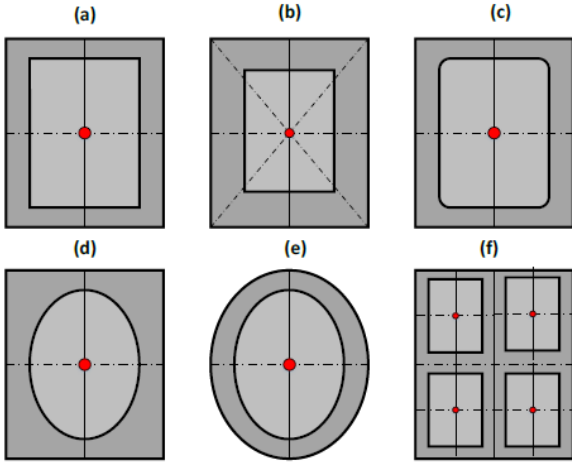


Figure I.7: Rectangular Pads [6].

➤ **Conical Pads**

Figure I.8 illustrates conical pads which require less pumping power.

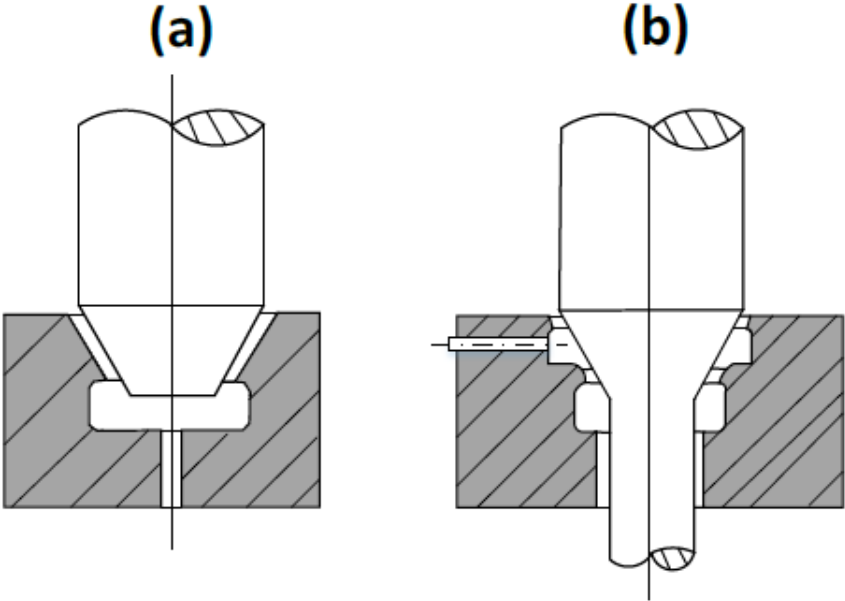


Figure I.8: Conical Pads [6].

**I.2.4.1.2 Multi-directional Pads:**

The bearings indicated in the figure below can support loads in two cases: loads in the axial direction and loads in the radial direction.

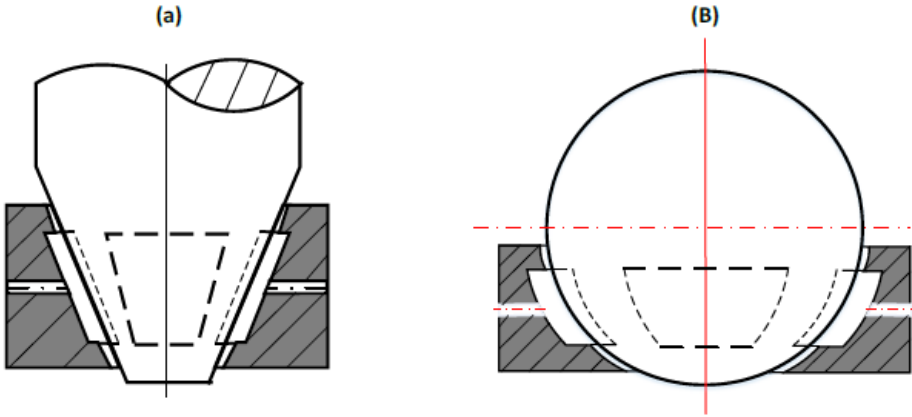


Figure I.9: Multi-directional Pads [6].

**I.2.4.1.3 Radial Pads:**

This figure depicts a cylindrical pad, which term is used in cases of hybrid bearings that can support loads only in the radial direction. In this type of pad:

- The rotational speed of the shaft is sufficiently high.
- A hydrodynamic pressure field superimposes on the hydrostatic field.

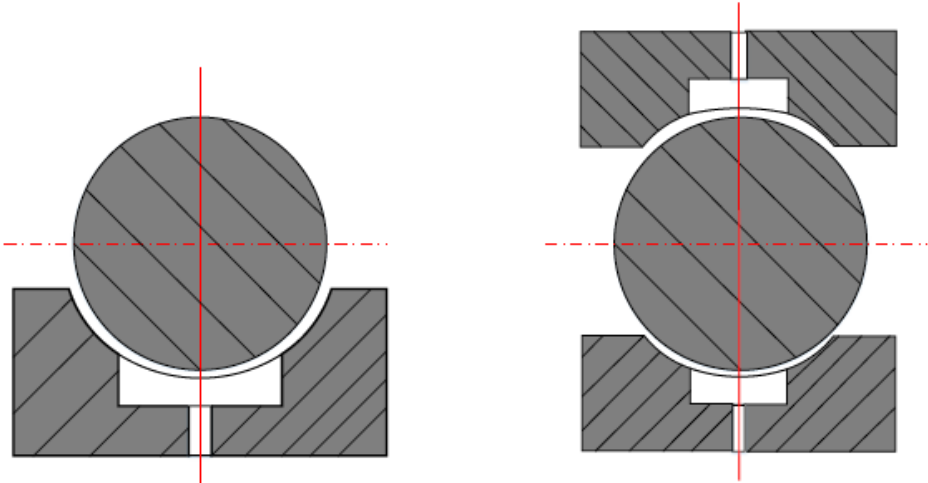


Figure I.10: Radial Pads [6].

**I.2.4.2 hydrostatic bearings with three pads:**

In Figure I.11, we have schematized a hydrostatic bearing with three pads. The indices 1, 2, and 3 indicate the characteristics corresponding to each pad, which, when assembled, form the three-pad hydrostatic bearing. These pads are supplied with fluid through the cavities, which are themselves supplied by an external pressure through hydraulic resistors. We assume that the depth of the cavities is sufficient to allow for the assumption of constant pressure.

The three-pad hydrostatic bearing consists of two parts:

A fixed part: represented by three identical pads, where each pad has a central cavity controlled and supplied by a hydraulic resistor of the orifice type.

A mobile part: represented by the movable journal (bearing).

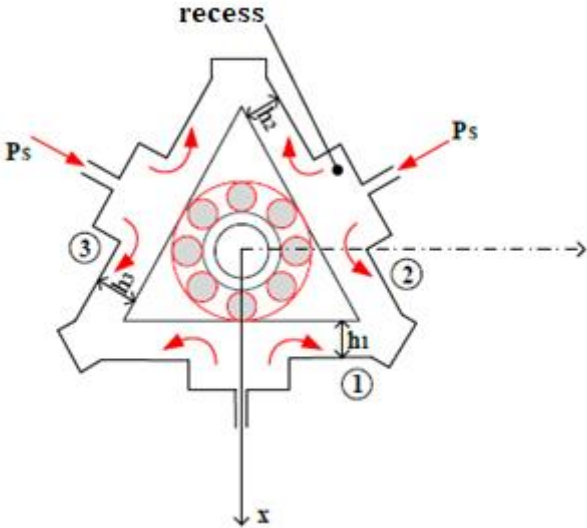


Figure I.11: Schematic representation of a three-pad hydrostatic bearing [24].

**I.2.4.3 Hydrostatic Four-Pad Bearing:**

Figure I.12 depicts a rolling bearing supported on a hydrostatic bearing consisting of four pads.

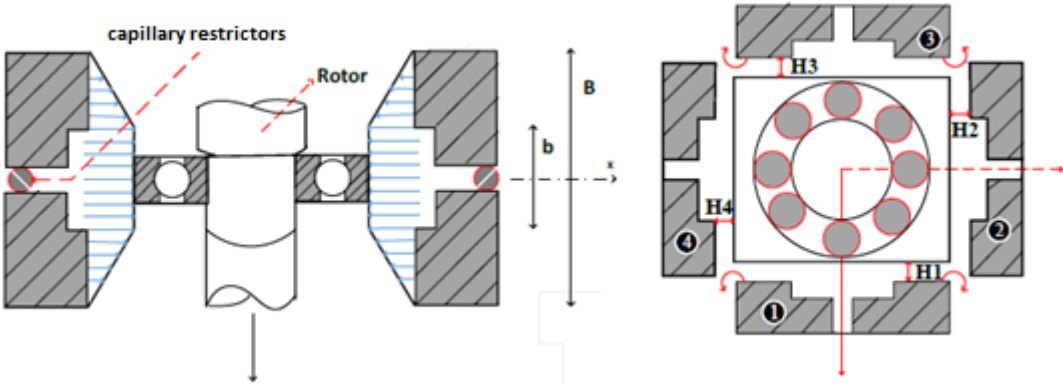


Figure I.12: Schematic representation of a four-pad hydrostatic bearing [24].

**I.2.4.4 The advantages and disadvantages of hydrostatic bearings:**

**Advantages:**

- A very high stiffness allowing for precise positioning despite significant load fluctuations;

- The presence of a lubricating film regardless of the speed of the surfaces, even at startup, there is no metal-to-metal contact; wear is therefore theoretically zero and the mechanism's lifespan is infinite;
- The absence of oil pressure variation because the pressure is substantially constant in the pocket and the load is supported by a large surface;
- The shape defects of the surfaces involved are less important than in hydrodynamic conditions because the pressure in the pocket depends on the overall flow rate and its geometry rather than the film thickness;
- Thermal problems are often secondary because we are dealing with a forced flow at a significant flow rate, thus, the assumption of an isothermal flow regime is justified.
- These advantages have been the subject of numerous studies that have allowed for a fairly good understanding of their behavior during operation.

### **Disadvantages:**

The major disadvantages of hydrostatic bearings are:

- Cost, as they require a pump, filters, pressure regulators, etc.
- Reliability, as even minor incidents in the supply system can lead to the destruction of surfaces. There is a wide variety of hydrostatic bearing geometries and potential strategies to control pressures.

### **I.2.4.5 Geometric characteristics of hydrostatic bearings:**

A hydrostatic bearing consists of  $n$  cavities distributed regularly around the periphery of the bearing. Two types of bearings exist depending on whether the cavities are decoupled or not by axial grooves. The latter have the advantage of decoupling the cavities and better irrigating the bearing. However, they increase the fluid flow rate and can introduce air into the bearing when the shaft rotation speed is very high [7].

#### **➤ Approximate calculation of the static characteristics of hydrostatic bearings:**

A hydrostatic bearing consists of  $n$  cavities distributed regularly around the periphery of the bearing. Two types of bearings exist depending on whether the cavities are decoupled or not by axial grooves. The latter have the advantage of decoupling the cavities and better irrigating the

bearing. However, they increase the fluid flow rate and can introduce air into the bearing when the shaft rotation speed is very high [7].

If the inter-cavity distance is small and in the absence of axial grooves, the circumferential flow can be neglected. Similarly, if the distance between the cavity and the edge of the bearing is small, the axial gradient can be assumed constant. This assumption is strictly verified if the film thickness is constant in the axial direction and if the flow regime is laminar. If a load is applied to the shaft, it moves inside the bearing until the resultant of the pressure forces balances the load. Depending on the direction of the load, the pressure distribution near a cavity may or may not be symmetrical, being influenced by the pressure in the cavities and the geometry of the fluid film. Analytical calculation of the performance of a hydrostatic bearing is difficult for the following reasons:

- \_ In a loaded bearing, the lubricating film thickness is not uniform;
- \_ There is inter-cavity flow.

### I.2.5 Hydrostatic lubrication:

#### I.2.5.1 Definition:

Hydrostatic lubrication is among the most widely used processes in the industrial domain and is defined as a lubrication system in which the load-supporting fluid film, separating the two surfaces, is created by an external source, such as a pump, supplying fluid under sufficient pressure. Therefore, hydrostatic bearings can operate at zero relative speed and very high load in the presence of an adequate thickness film (hence the name "Hydrostatic") [8].

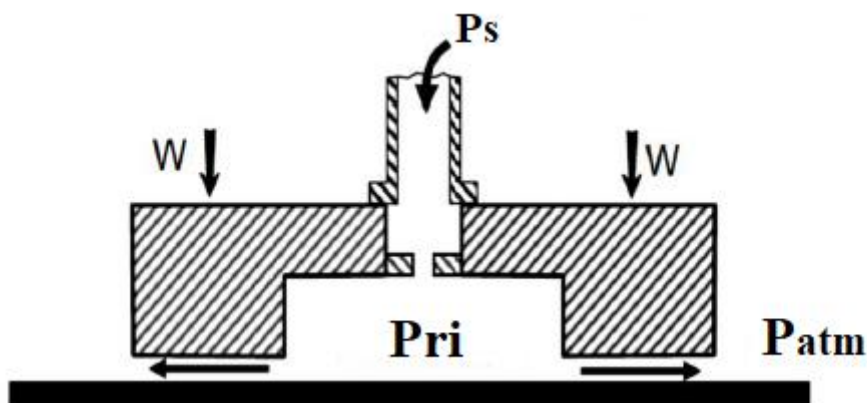


Figure I.13: Rheological behavior of time-dependent fluids [8].

### I.2.5.2 Principle of hydrostatic lubrication:

A hydrodynamic bearing has the drawback of only operating in a fluid friction state when the speed is sufficiently high. To create the fluid film even at rest, the lubricant is pressurized and injected using a pump into cavities (Figure I.14) where it creates pressure that lifts the load; it then escapes through the grooves.

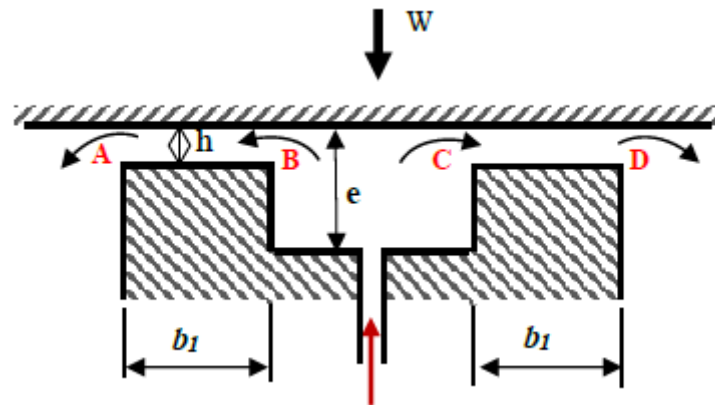


Figure I.14: Schematization of a hydrostatic thrust bearing [8].

The thickness of the film adjusts automatically according to the applied pressure and load. It is necessary to provide restrictions in the fluid supply pipes to the pads to stabilize the position of the moving part.

Two regions illustrate the operating principle of a hydrostatic thrust bearing, one area represented by the surfaces (AB) and (CD) with a width ( $b_1$ ) where the thickness ( $h$ ) of the lubricating film is thin:  $h/a < 1$ . The area (BC) consists of the cavity where the thickness of the lubricating film ( $e$ ) is large:  $e/h > 20$ ; in this region, the pressure is assumed to be constant:  $p = p_a$ ; this assumption is often experimentally verified.

There are two methods to introduce the fluid into the pads:

- Constant pressure systems: In mechanisms with constant pressure, a hydraulic resistance is placed immediately upstream of the recess. The role of this resistance is to create a pressure drop, i.e., to control the flow rate with the pressure drop. This system, simple to implement, allows several recesses to be supplied with a single pump provided, of course, that its flow rate is sufficient (Figure. I.15).

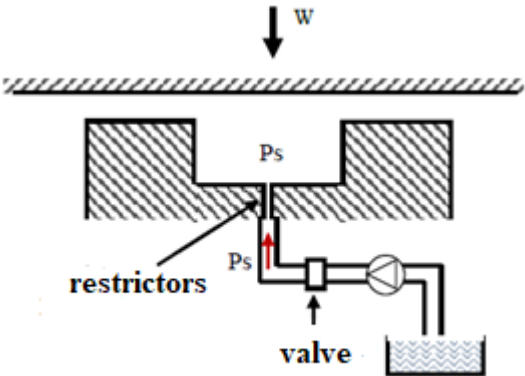


Figure I.15: Constant pressure supply [8].

- Constant flow systems: In constant flow systems, a constant flow pump is placed between the reservoir and the recess. This system is rarely used because, when the mechanism has several recesses (which is practically always the case), it is necessary either to supply each of them with an individual pump or to use constant flow regulators. This solution, which ensures high stiffness, is complex and expensive (Figure. I.16).

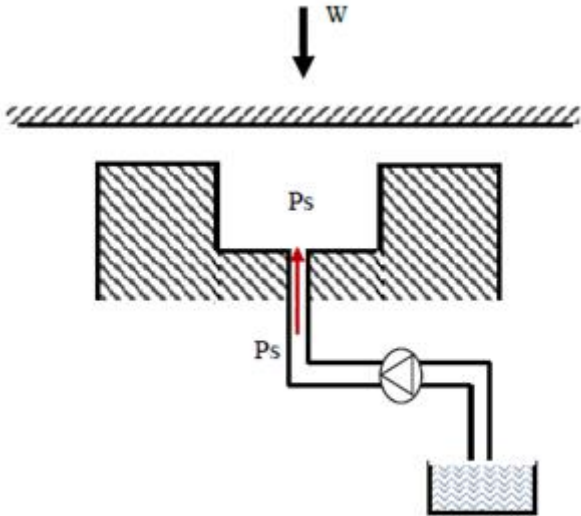


Figure I.16: Constant flow supply [8].

I.2.5.3 Formation of the hydrostatic fluid film:

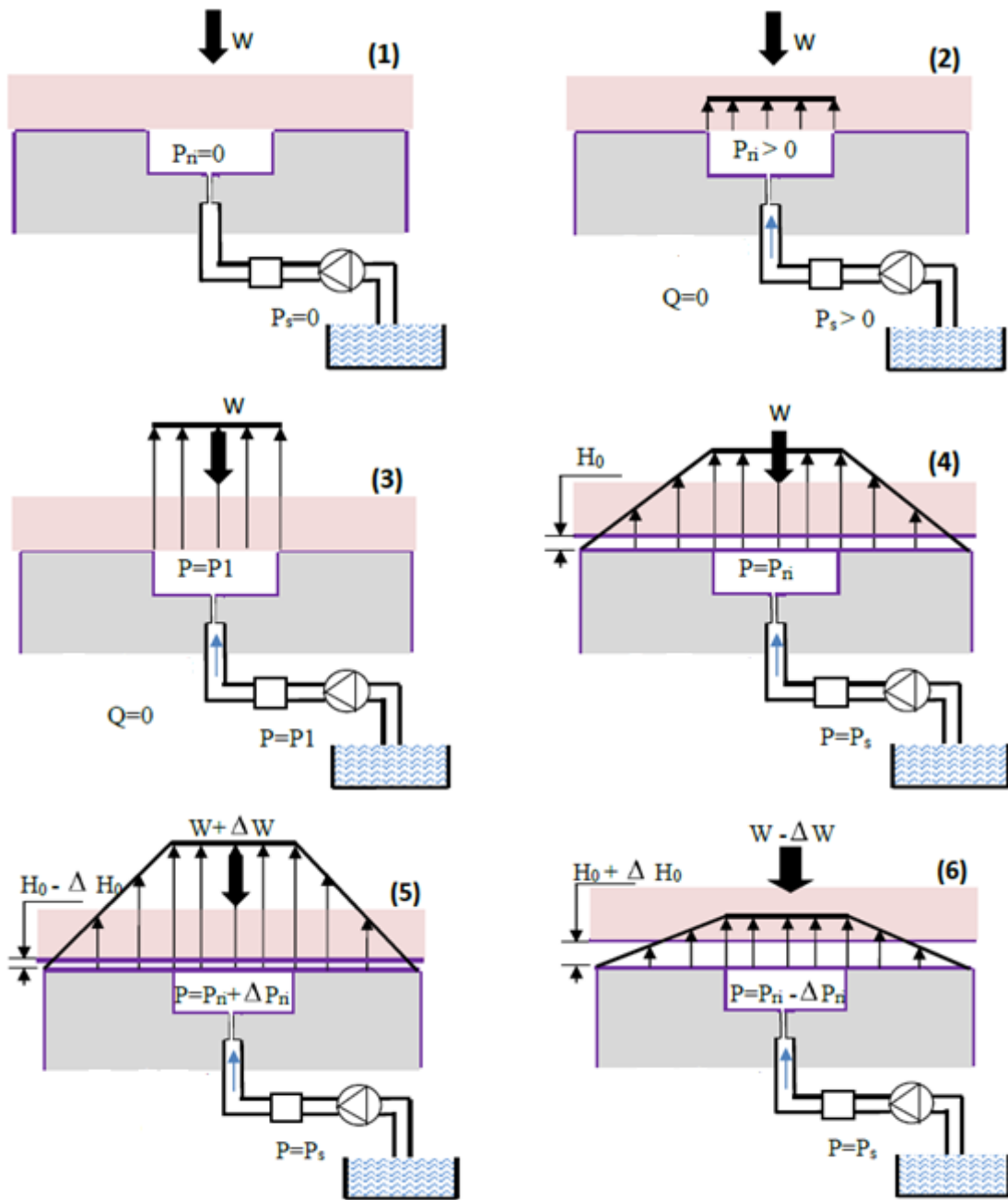


Figure I.17: Formation of the fluid film in a hydrostatic thrust bearing [8].

- 1) The pump is in a stopped state;
- 2) Pressurized fluid begins to flow towards the thrust bearing, and the pressure in the recess increases;
- 3) The recess pressure increases until the pressure across the recess surface is sufficient to lift the applied load;
- 4) The bearing starts to operate, the fluid flows through the system, and a pressure drop exists between the pressure source and the pad, and between the recess and the pad outlet;

5) As the load increases, the film thickness decreases, and the recess pressure increases until the pressure integrated across the bearing surfaces equals the applied load;

6) When the load decreases, the film thickness increases, and the recess pressure decreases.

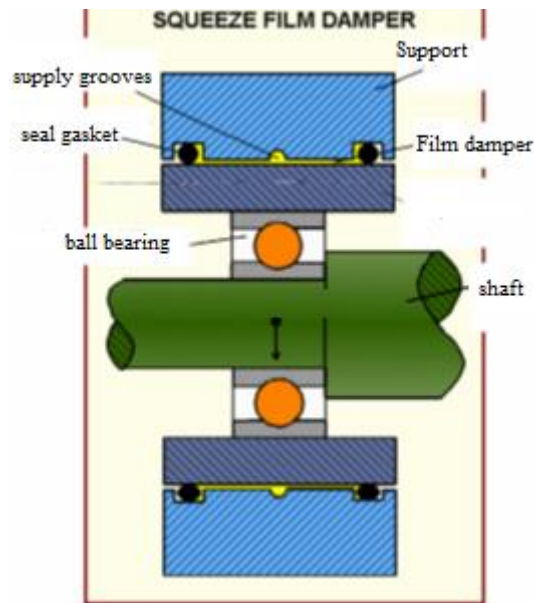


Figure I.18 Schematic diagram of a damping film bearing (SFD) [7].

#### **I.2.5.4 Hydraulic Resistances:**

- **Capillary-Type Hydraulic Resistance**

If the flow regime in the capillary is laminar:

- It provides stiffness independent of the viscosity of the fluid, as viscosity is related to flow rate.

- It is also easier to calibrate.

The flow rate:  $Q_{ri} = \frac{\pi d_c^4}{128 \mu l_C} (P_s - P_{ri})$  or  $R_p = \frac{\rho U_c d_c}{\mu} < 1000$  and  $U_c = \frac{Q_r}{(\pi d_c^2 / 4)}$  (I.1)

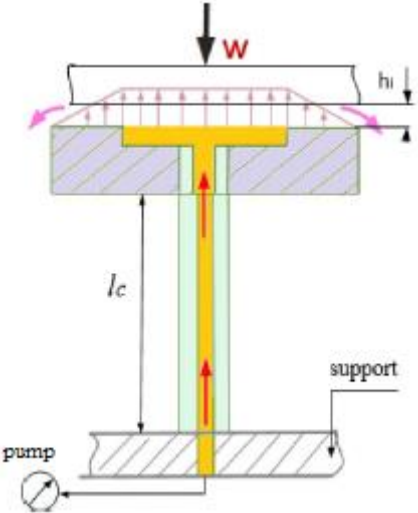


Figure I.19 Capillary-Type Hydraulic Resistance [9].

- **Hydraulic resistance of orifice type**

Advantages of orifices in a non-laminar regime:

- \_ High stiffness.
- \_ Reduced space requirements.

The flow rate:

$$Q_{ri} = \frac{\pi c_d d_0^2}{4} \left[ \frac{2(P_s - P_{ri})}{\rho} \right]^{\frac{1}{2}} \tag{I.2}$$

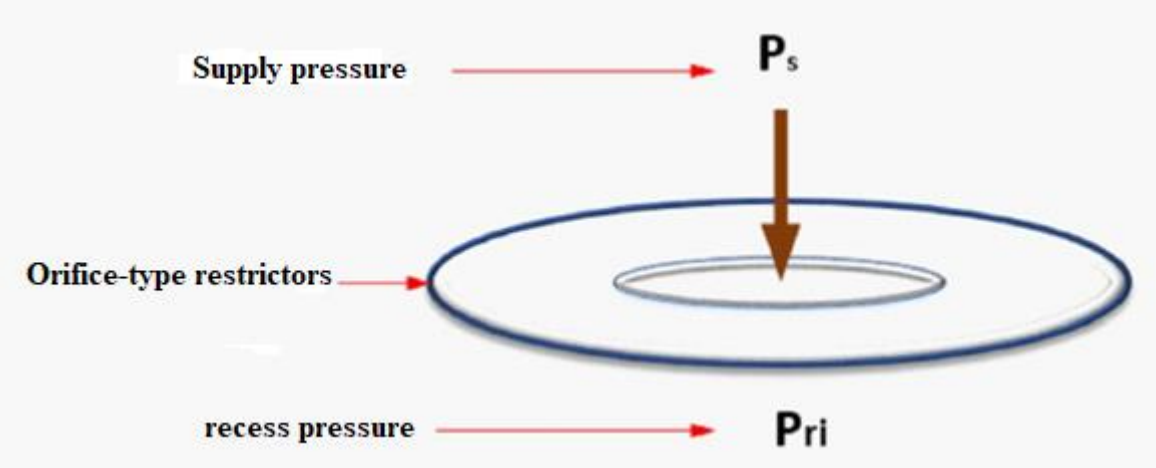


Figure I.20 Hydraulic resistance of orifice type [9].

### I.3 Lubricants

#### ➤ Mineral-based oils

It is divided into the paraffin structure of saturated linear hydrocarbons (very stable to oxidation and good high temperature resistance) and the naphthenic structure of the ring (very suitable for gelation).

#### ➤ Synthetic-based oils

It has several types, such as phosphorus, aliphatic, widely appreciated for its low viscosity and low freezing point at low temperatures, and polypropylene glycol.

#### I.3.1 Newtonian Fluid:

A Newtonian fluid is composed of simple molecules.

The shear stress is proportional to the velocity gradient:

- \_ In a simple shear flow, the only stress generated by the flow is the shear stress.
- \_ Viscosity has nothing to do with the shear rate.
- \_ Viscosity has nothing to do with time. When the flow stops, stresses immediately cancel out.

#### I.3.2 Non-Newtonian Fluid:

Any deviation from Newtonian fluid rules indicates non-Newtonian behavior. Describing these behaviors and interpreting them in relation to the fluid's microstructure constitute a discipline called rheology. This field has only recently emerged, but with the advent of synthetic polymers, it has experienced considerable development. The most common non-Newtonian property is the change in viscosity with shear rate. Generally, for polymer solutions, viscosity decreases as the shear rate (velocity gradient) experienced by the fluid increases. This is known as shear-thinning behavior in rheofluids.

#### I.3.3 Complex Fluid:

A fluid can be termed complex when it possesses an internal structure with a characteristic size ranging between the molecular scale and that of the sample. These mesoscopic sizes (intermediate dimensions between those of quantum physics and classical physics) impart to fluids a microstructure that gives them very particular and sometimes very surprising properties. These properties lie between those of a simple fluid and purely elastic solids. Due to their unique properties, these products play a role in everyday life, as well as serving as finished or

intermediate products in most process industries. Listing all industrial sectors where complex fluids are used is a challenge; however, from heavy industries to the finest ones, the most particularly affected areas include: drilling muds in oil field exploitation, cements and mortars, ore treatment in extractive metallurgy, molten polymers, paper pulp, mastics, paints and varnishes, food industries (ketchup, mayonnaise...), cosmetics, and pharmaceuticals.

Commercialized fracturing fluids are non-Newtonian fluids with complex rheological behavior that enables better transport of proppants. The code previously developed for Newtonian fluids is adapted to complex fluids. Changes need to be made in the suspension viscosity, which depends on both particle concentration and shear rate.

The vast majority of fracturing fluids exhibit shear-thinning behavior (viscosity increases as shear rate decreases), thus countering sedimentation at low shear rates.

The complex rheological behavior of the carrier fluid allows the development of regions with high viscosity, slowing down particle sedimentation and making particle transport more efficient.

### **I.3.4 Micropolar Fluids:**

Micropolar fluids are fluids with microstructures. They belong to a class of fluids with nonsymmetrical stress tensors which we will refer to as polar fluids, and include, as a particular case, the well-known Navier-Stokes model of classical fluids, which we will call ordinary fluids. Physically, micropolar fluids can represent fluids composed of rigid particles, randomly oriented (or spherical) suspended in a viscous medium, with the deformation of fluid particles being ignored [10].

The model of micropolar fluids introduced by C.A. Eringen [11] is worth studying as it is very well balanced. Firstly, it is a meaningful and significant generalization of the classical Navier-Stokes model, covering both in theory and applications many more phenomena than the classical model. Furthermore, it is elegant and not too complicated, in other words, manageable for mathematicians studying its theory and for physicists and engineers applying it. The lubrication theories applied to the analysis of bearings by various researchers have only taken into account the macroscopic modification of lubricant properties. Individual particles in the lubricant can change their shape or movement and become effective in the equivalent region of bearing clearances. Therefore, the classical Newtonian postulate is not valid for fluids considering the effect of molecules. Newtonian fluid mechanics must be generalized when the

outer length scale becomes comparable to the average dimensions of material particles in complex fluids such as polymeric suspensions, animal blood, and liquid crystals. The presence of microstructures in the fluid can be felt in several ways; in the case of liquid crystals, for example, their orientation impacts overall flow. These microstructures can also have their own angular velocity, leading to the emergence of new stresses that must be taken into account.

### **I.3.5 Micropolar Lubrication:**

#### **I.3.5.1 Definition:**

Lubrication is a set of techniques used to reduce friction and wear between two elements in contact and moving against each other. In general, some of the heat generated by friction can be dissipated, and corrosion can be prevented. In these cases, the flow of the fluid is parallel to the surface, which simplifies their description and calculation (lubrication theory). We talk about lubrication when the lubricant (mechanical) is liquid and we talk about lubrication when the lubricant is solid. Micropolar fluids [11] arise from a simplification of the microfluidics theory [12] from 22 viscosity coefficients to 6 viscosity coefficients ( $\alpha$ ,  $\beta$ ,  $\gamma_v$ ,  $k_v$ ,  $\mu$ , and  $\lambda$ ) considering non-deforming microstructures with no inherent orientation, thus retaining only the effects due to their rotation, where a new particle angular velocity vector and the corresponding viscosity coefficients have been added to the Navier-Stokes equations. This constitutes a substantial generalization of these equations and opens up a new field of applications including a large number of complex fluids. The application of the micropolar fluid model in many classic cases is straightforward, such as flow through a capillary or between two parallel plates under the usual geometric and dynamic assumptions. The simplicity of the micropolar fluid model obviously does not mean mathematical triviality. The classical Navier-Stokes model itself is a particular case of the micropolar fluid model and is far from trivial; in this context, simplicity means the elegance and beauty of mathematical theory.

#### **I.3.5.2 Some application of micropolar lubrication:**

Theoretical investigations into micropolar lubrication of bearings were initiated by Allen [10]. They found that the load-carrying capacity of an inclined bearing increases and its friction coefficient decreases with a micropolar lubricant.

SHUKLA et al [11] studied the film thickness profile to maximize the load-carrying capacity. This analysis revealed that the maximum load increases as the parameter characterizing the microstructure of the suspension increases.

PRAKASH et al [12] proposed an infinitely long bearing with micropolar lubricants. They found that these fluids increase dynamic viscosity, especially in the presence of thin films.

ZAHEERUDDIN et al [13] studied infinitely long bearings as well as infinitely short bearings operating with micropolar lubricants. The study showed that compared to Newtonian lubricants, micropolar lubricants can increase bearing load and friction torque while reducing the friction coefficient. Similar effects were found by TIPEI [14] with short bearings. A detailed study by SINGH et al [15] focused on the three Reynolds equations for micropolar lubrication.

In 2005 [16], Gay Bayada, Nadia Benhaboucha, Michèle Chambat conducted a study on a thin micropolar fluid with new boundary conditions at the fluid-solid interface, linking velocity and micro-rotation by introducing a 'limiting viscosity'. The existence and uniqueness of the solution are proven.

In 2007, Bouzidane [9] studied a hydrostatic bearing with four hydrostatic pads supplied by an electro-rheological fluid, to control vibrations of flexible rotors during critical speed transitions.

### **I.3.5.3 Equations of Micropolar Lubrication:**

The equations for compressible micropolar fluid are proposed by Eringen in vector form:

Mass Conservation:

$$\frac{\partial \rho}{\partial t} + \nabla \cdot (\rho V) = 0 \quad (I.3)$$

Conservation of Linear Momentum:

$$-\nabla P + (\lambda + 2\mu) \nabla \nabla \cdot V + k_v \nabla \times \omega - \left( \mu + \frac{k_v}{2} \right) \nabla \times \nabla \times V + \rho f_v = \rho \frac{DV}{Dt} \quad (I.4)$$

Conservation of Angular Momentum:

$$(\alpha + \beta + \gamma_v) \nabla \nabla \cdot \omega - \gamma_v \nabla \times \nabla \times \omega + k_v \nabla \times V - 2k_v \omega + \rho f_c = \rho j \frac{D\omega}{Dt} \quad (I.5)$$

It should be noted that the system (I.1-I.3) consists of 7 equations for the 7 functions P(x, y, z).

$$V = (u_1(x, y, z), u_2(x, y, z), u_3(x, y, z)) \text{ et } \omega = (\omega_1(x, y, z), \omega_2(x, y, z), \omega_3(x, y, z)) \quad (I.6)$$

$\mu$  and  $\lambda$  are the viscosity coefficients of the Newtonian fluid. The volumetric forces are grouped here under the term  $f_v$ ; these are forcing whose effect is expressed over distances. The volumetric force  $f_c$  is a torque force, which appears, for example, when the domain is in rotation.  $\omega$  is the rotation vector.  $\rho$  is the density.  $V$  is the velocity vector.  $P$  is the static pressure.  $j$  represents the characteristic dimension of the microstructures composing a micropolar fluid. Some authors call this latter the microinertia coefficient, while others call it the gyration radius.

The compressible nature of the fluid is characterized by the first equation. If we consider an incompressible fluid, equation (I.3) becomes  $\nabla \cdot V = 0$ . This relationship indicates that if a quantity of matter enters a given volume, an equivalent quantity must exit.

The right-hand side of equation (I.4) expresses the total variation of the velocity field  $V$  with respect to time.

$$\frac{DV}{Dt} = \frac{\partial V}{\partial t} + V \cdot \nabla V \quad (I.7)$$

The variation of linear momentum depends on two types of forces acting on the fluid: surface forces and volumetric forces.

Surface forces are represented by three terms: the term  $-\nabla P$ , which quantifies normal forces, and the viscous term  $(\lambda + 2\mu)\nabla \nabla \cdot V$ , which arises from shear effects. The third term  $k_v \nabla \times \omega - (\mu + k_v / 2)\nabla \nabla V$  is new; it represents the effects produced by the rotation of microstructures.

This new term contains a difference between the gyration  $\omega$  and the local angular velocity. Thus, if the gyration induced by the rotation of microstructures has the same intensity and direction as the local angular velocity of the fluid, this term cancels out. The impact of microstructures on the flow is then null. On the other hand, a difference between the direction or intensity of the rotation of microstructures and the angular velocity of the fluid leads to a modification of the velocity field.

Equation (I.5) describes the evolution of gyration, considering the total variation of this variable

$$\frac{D\omega}{Dt} = \frac{\partial \omega}{\partial t} + V \cdot \nabla \omega \quad (I.8)$$

To account for the different rotation effects, we introduce four new coefficients:  $\alpha$ ,  $\beta$ ,  $\gamma_v$ , and  $k_v$ . For the first two coefficients ( $\alpha$  and  $\beta$ ), no clear physical interpretation has been given.  $\gamma_v$  is a viscosity coefficient of the micropolar fluid. The coefficient  $k_v$  facilitates the exchange of angular momentum between the medium and the microstructures; some authors [19]; [20] refer to this coefficient as 'the spin viscosity'.

### I.3.5.4 Hypothesis and Demonstration:

To establish the modified Reynolds equation for an incompressible micropolar fluid, we make the following assumptions:

1. All characteristic coefficients are independent.
2. Torque forces and volumetric forces are neglected.
3. The film is thin enough compared to the length and span of the bearing to allow the curvature of the fluid film to be ignored.
4. The flow is laminar: vortex and turbulence do not occur in the film.
5. There is no slip on the bearing surfaces.

Three additional assumptions are made:

1. The bearing surfaces are smooth, meaning there is no surface roughness.
2. The bearing surfaces are non-porous.
3. The bearing surfaces are rigid, meaning they are not deformed under fluid pressure.

Now, let's suppose that the velocity and gyration have the following form:

$$V = (u_1, u_2, u_3) \text{ et } \omega = (\omega_1, 0, \omega_3) \quad (\text{I.9})$$

We obtain the following differential equations for the lubricant flow:

$$\frac{1}{2}(2\mu + k_v) \frac{\partial^2 u_1}{\partial y^2} + k_v \frac{\partial \omega_3}{\partial y} - \frac{\partial p}{\partial x} = 0 \quad (\text{I.10})$$

$$\frac{1}{2}(2\mu + k_v) \frac{\partial^2 u_3}{\partial y^2} + k_v \frac{\partial \omega_1}{\partial y} - \frac{\partial p}{\partial x} = 0 \quad (\text{I.11})$$

$$\gamma_v \frac{\partial^2 \omega_3}{\partial y^2} - k_v \frac{\partial u_1}{\partial y} - k_v \cdot \omega_3 = 0 \quad (\text{I.12})$$

$$\gamma_v \frac{\partial^2 \omega_1}{\partial y^2} - k_v \frac{\partial u_3}{\partial y} - k_v \cdot \omega_1 = 0 \quad (\text{I.13})$$

$$\frac{\partial u_1}{\partial x} + \frac{\partial u_2}{\partial y} + \frac{\partial u_3}{\partial z} = 0 \quad (\text{I.14})$$

$$\frac{\partial p}{\partial y} = 0 \quad (\text{I.15})$$

For the lubricant layer (Figure I.10), the boundary conditions are as follows:

$$y = 0 \begin{cases} u_1 = U_1 \\ u_2 = 0 \\ u_3 = 0 \end{cases}, \omega_1 = \omega_2 = \omega_3 = 0 \quad (\text{I.16})$$

$$y = h \begin{cases} u_1 = U_2 \\ u_2 = V_2 + U_2 \frac{\partial h}{\partial x} \\ u_3 = 0 \end{cases}, \omega_1 = \omega_2 = \omega_3 = 0 \quad (\text{I.17})$$

Where  $h$  represents the thickness of the oil film,  $U_1$  is the tangential velocity of surface 1,  $U_2$  and  $V$  are the tangential and normal velocities of surface 2, respectively.

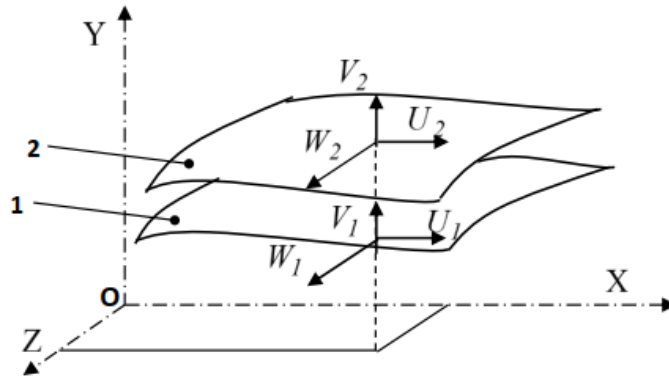


Figure I.21: Geometry and Kinematics of Contact [24].

The expressions for the velocities  $u_1$ ,  $u_3$  and the angular velocities of the microstructures  $\omega_1$ ,  $\omega_3$  resulting from the solution of equations (I.7-I.12), taking into account the boundary conditions (I.13), are:

$$U_1 = \frac{1}{\mu} \frac{\partial P}{\partial x} \left[ \frac{y^2}{2} - \frac{N^2 h}{m} \frac{ch(m y) - 1}{sh(m h)} \right] + U_1 + \frac{D_1}{1 - N^2} \left( y - \frac{N^2}{m} \left[ sh(m y) - \frac{(ch(m y) - 1)(ch(m h) - 1)}{sh(m h)} \right] \right) \quad (I.18)$$

$$U_3 = \frac{1}{\mu} \frac{\partial P}{\partial z} \left[ \frac{y^2}{2} - \frac{N^2 h}{m} \frac{ch(m y) - 1}{sh(m h)} \right] + \frac{D_2}{1 - N^2} \left( y - \frac{N^2}{m} \left[ sh(m y) - \frac{(ch(m y) - 1)(ch(m h) - 1)}{sh(m h)} \right] \right) \quad (I.19)$$

$$\omega_1 = - \left[ \frac{D_2}{2(1 - N^2)} (ch(m y) - 1) + \frac{sh(m y)}{sh(m h)} \left[ \frac{h}{2\mu} \frac{\partial P}{\partial z} - \frac{D_2}{2(1 - N^2)} ch(m h) - 1 \right] - \frac{1}{2\mu} \frac{\partial P}{\partial z} y \right] \quad (I.20)$$

$$\omega_3 = \frac{D_1}{2(1 - N^2)} (ch(m y) - 1) + \frac{sh(m y)}{sh(m h)} \left[ \frac{h}{2\mu} \frac{\partial P}{\partial z} - \frac{D_1}{2(1 - N^2)} ch(m h) - 1 \right] - \frac{1}{2\mu} \frac{\partial P}{\partial x} y \quad (I.21)$$

Or:

$$D_1 = - \frac{(1 - N^2)}{2} \left( \frac{h}{\mu} \frac{\partial P}{\partial x} + (U_1 - U_2) \left[ \frac{h}{2} - \frac{N^2}{m} \frac{ch(m h) - 1}{sh(m h)} \right] \right) \quad (I.22)$$

$$D_2 = - \frac{(1 - N^2)}{2} \frac{h}{\mu} \frac{\partial P}{\partial z} \quad (I.23)$$

$$N = \left( \frac{k_v}{2\mu + k_v} \right)^{0.5} ; l_m = \left( \frac{\gamma_v}{4\mu} \right)^{0.5} ; m = \frac{N}{l_m} \quad (I.24)$$

N and  $l_m$  are two parameters that characterize a micropolar fluid relative to a Newtonian fluid. N characterizes the coupling of the equation of linear momentum and the equation of angular momentum, and it is called the "coupling number".  $l_m$  Characterizes the length of the micropolar fluid element. This parameter can be identified as the size of the microstructures present in the lubricant.

Now, by integrating the continuity equation (I.11) along y, we obtain:

$$V_2 = -\left(\frac{\partial}{\partial x} \int_0^h u_1 \partial y + \frac{\partial}{\partial z} \int_0^h u_3 \partial y + u_2 \frac{\partial h}{\partial x}\right) \quad (\text{I.25})$$

Then, by substituting  $u_1$  and  $u_3$  from equation (I.14), (I.15), and considering  $V_2$  as the crushing velocity, that is,  $V_2 = \frac{\partial h}{\partial t}$  we obtain the modified Reynolds equation for the micropolar fluid:

$$\frac{\partial}{\partial x} \left[ G(h, l_m, N) \frac{\partial p}{\partial x} \right] + G(h, l_m, N) \frac{\partial^2 p}{\partial z^2} = 12 \frac{\partial h}{\partial t} + 6(U_1 + U_2) \frac{\partial h}{\partial x} \quad (\text{I.26})$$

With:

$$G(h, l_m, N) = \frac{h}{\mu} \left[ h^2 + 12l_m^2 - 6Nl_m h \frac{1 + ch(Nh/l_m)}{sh(Nh/l_m)} \right] \quad (\text{I.27})$$

When  $l_m$  is set to zero, Equation I.26 reduces to the classical form of the Reynolds equation.

#### **I.4 The dynamics of the rotors:**

The dynamic of rotors is the study of the dynamics and stability of rotating machines. It plays an important role in improving the security and performance of these systems. As the speed of rotation of a rotating object increases, its vibration level often crosses a threshold, its critical speed. This evolution is often excited by an imbalance of the rotating structure. If the amplitude of the vibration at these critical speeds becomes excessive, a catastrophic failure can occur. A turbomachine can also develop instabilities related to its internal construction, also leading to catastrophic failures. For the engineer who designs large rotors, having to resort only to expensive prototypes and physical tests is a real handicap [21].



Figure I.22: An example of a rotor [22].

### **I.4.1 Predictions of the dynamic behavior of rotors:**

A rotor system can consist of discs and blades of different shapes, different diameters of the shafts and bearings located in different positions the rotors of rotating machines are classified according to their characteristics, as follows:

#### **➤ Rigid rotor:**

If the deformation of the rotating shaft is negligible in the operating speed range, it is called a rigid rotor.

#### **➤ Flexible Rotor:**

A rotor is generally considered to be soft or flexible when it operates close to or above its natural frequency (critical speed). The basic rule is to consider a flexible rotor if it runs at 70% of the 1st critical or faster. If the shaft begins to deform noticeably at the beginning of the operating speed range, it is called a flexible rotor [23].

### **I.4.2 Objectives of the dynamic analysis of rotors:**

During the design, operation and maintenance of rotating machines, the dynamic analysis of rotors can help to achieve the following objectives:

- 1- Predict the critical speeds. Speeds at which the vibrations due to the imbalance of the rotor are maximum.

2- Determine the design modifications to change the critical speeds. it becomes necessary to modify the operating speed range of a machine, design modifications may be necessary to change the critical speeds.

3- Predict the natural frequencies of vibration in torsion, bending and coupling.

4- Calculate the values and the positions of the masses of the correction unbalance, in a balancing operation, from the measured vibration data.

5- Provide for synchronous vibration amplitudes caused by the imbalance of the rotor.

6- Predict speeds and vibration frequencies of dynamic instability threshold.

7- Determine the design changes to remove dynamic instabilities.

### **I.5 Conclusion:**

In summary, this first chapter has outlined essential aspects to understand the dynamic behavior of hydrostatic bearings. By exploring the classification of bearings, hydrostatic lubrication, micropolar fluids, and rotor dynamics, we have laid the necessary foundations for our in-depth study. By grasping these key concepts, we are now better equipped to tackle the challenges and opportunities related to the design and optimization of hydrostatic bearings in the upcoming chapters.

## **Chapter II**

# **Hydrostatic Bearing with four pads Lubricated by a Micropolar Fluid.**

### **II.1 Introduction:**

In this chapter, we delve into the mathematical modeling of hydrostatic bearings with four pads lubricated by micropolar fluids. Micropolar fluids exhibit unique flow characteristics due to internal rotational motion of their particles, which can significantly influence bearing performance.

We will formulate the governing equations for micropolar fluid lubrication, considering the hydrodynamic behavior of the bearing. The focus will be on deriving pressure distribution, film thickness, and load-carrying capacity, essential for understanding and optimizing the bearing's performance.

Numerical methods will be introduced for solving these equations, providing insights into the dynamic behavior of the bearing under various operating conditions. This mathematical framework serves as a foundation for our subsequent numerical analysis and optimization in the following chapters.

### **II.2 Study of a hydrostatic squeeze film damper:**

Figure II.1 shows a rolling bearing supported on a hydrostatic bearing used as an (HSFD) consisting of four pads. As shown in this illustration, all pads are identical. Indices 1, 2, 3, and 4 respectively refer to the characteristics of the lower, right, upper, and left hydrostatic flat pads. The HSFD is supplied with a micropolar lubricant through recesses in the bearing. These are supplied by an external pressure  $P_s$  through capillary-type hydraulic resistors.

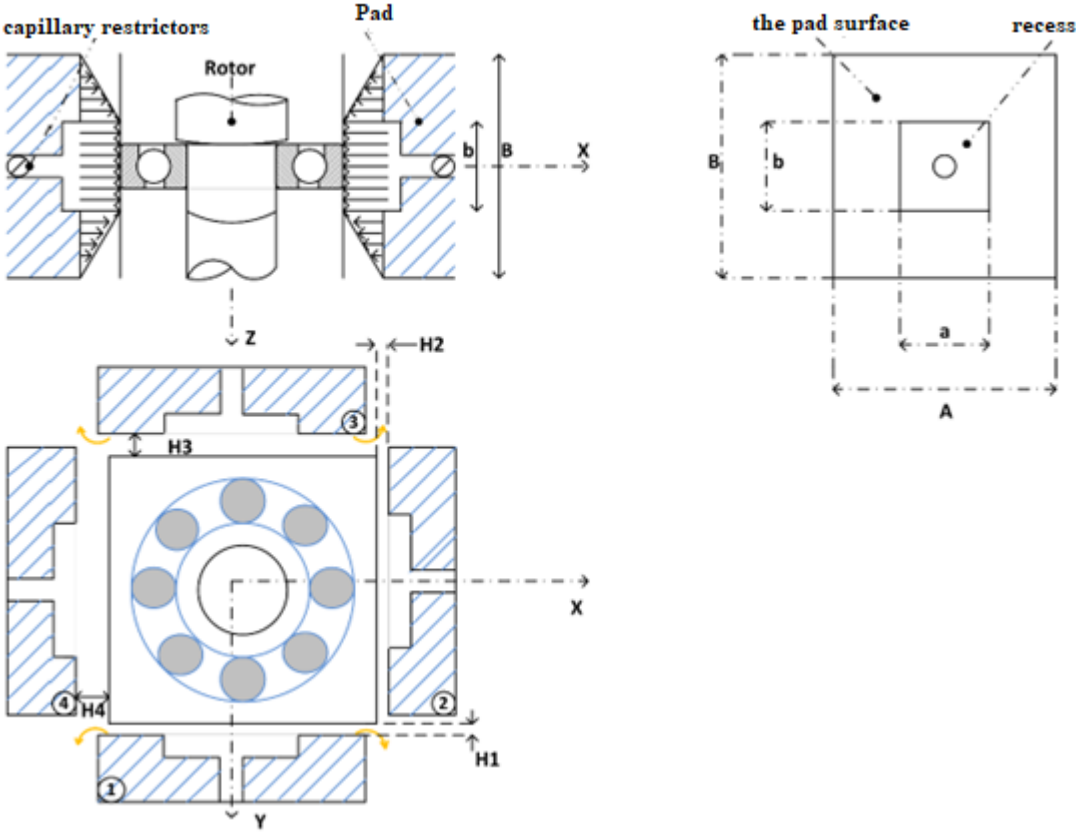


Figure II.1 Hydrostatic squeeze film damper geometry [24].

Where:

$h_i$ : represents the thickness of the lubricating film relative to the single-acting thrust bearing

No. i.

$\dot{h}_i$ : represents the squeeze velocity of the movable grain relative to the single-acting thrust

bearing No. i.

Figure II.2 shows a single-acting hydrostatic thrust bearing No. i, which is composed of a fixed part called the pad with a central recess and a movable part which is the rolling bearing. The latter is movable and driven by a linear velocity  $\dot{h}$ .

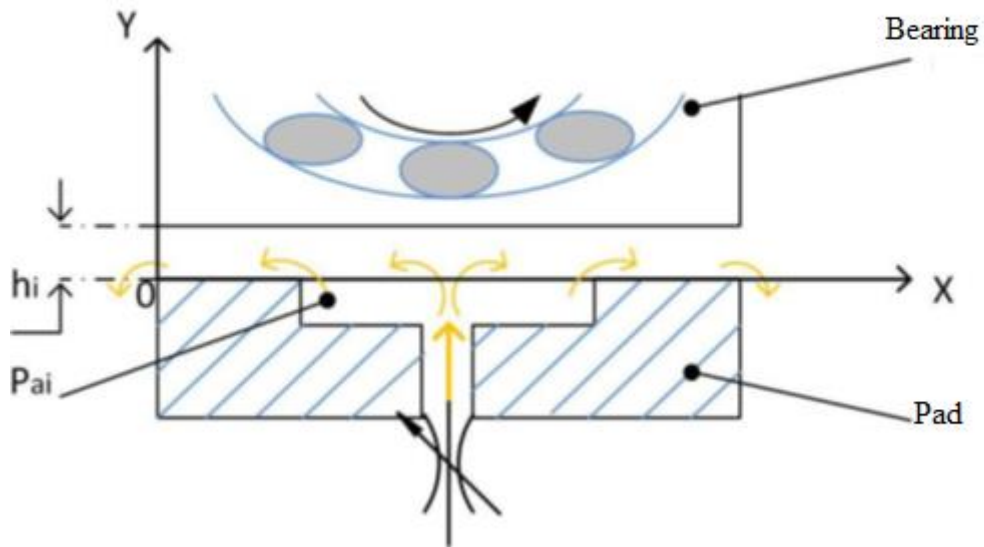


Figure II.2 Diagram of a single-acting hydrostatic thrust bearing [24].

Let  $h_0$  be the thickness of the film in the centered position:

The thickness of the film of the single-acting hydrostatic thrust bearing #1:

$$h_1 = h_0 - e_y \quad (\text{II.1})$$

The thickness of the film of the single-acting hydrostatic thrust bearing #2:

$$h_2 = h_0 - e_x \quad (\text{II.2})$$

The thickness of the film of the single-acting hydrostatic thrust bearing #3:

$$h_3 = h_0 + e_y \quad (\text{II.3})$$

The thickness of the film of the single-acting hydrostatic thrust bearing #4:

$$h_4 = h_0 + e_x \quad (\text{II.4})$$

Where  $e_x$  and  $e_y$  are the eccentricities in the x and y directions respectively.

### II.2.1 The modified Reynolds equation:

Solving the Reynolds equation allows us to calculate the pressure distribution. The work below demonstrates obtaining the solution to this equation using the finite difference method. The procedure incorporates the following assumptions: a) there is no slip between the fluid and the bearing pads, and b) the boundary conditions associated with the velocity field are represented in (Figure II.3):

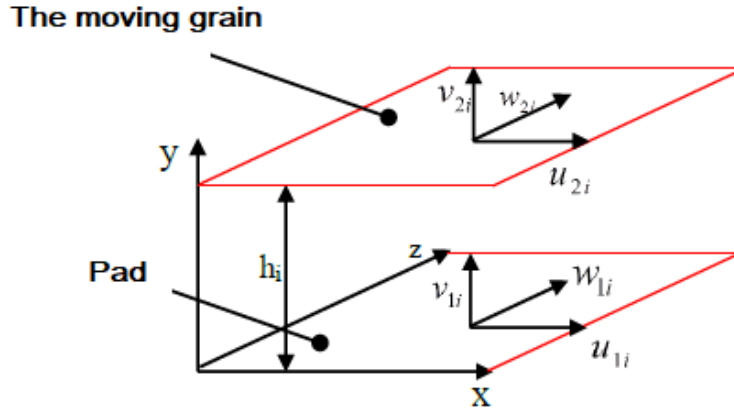


Figure II.3: Boundary conditions of a hydrostatic thrust bearing [29].

On the pad ( $y = 0$ ) :  $u_{1i} = 0; v_{1i} = 0 ; w_{1i} = 0$

On the moving grain ( $y = h_i$ ) :  $u_{2i} = 0; v_{2i} = \dot{h}_i ; w_{2i} = 0$

where:

$u_{1i}$ ,  $v_{1i}$ , and  $w_{1i}$  are respectively the surface velocities of the pad relative to the single-acting thrust bearing  $i$ th in the X, Y, and Z directions.

$u_{2i}$ ,  $v_{2i}$  and  $w_{2i}$  are respectively the surface velocities of the moving grain relative to the single-acting thrust bearing  $\#i$  in the X, Y, and Z directions.

With these conditions and for an incompressible, laminar, and isoviscous fluid, the modified Reynolds equation for a micropolar fluid (I.26) can be written as:

$$\frac{\partial}{\partial x_i} \left( G(\dot{h}_i, l_m, N) \frac{\partial p_i}{\partial x_i} \right) + G(\dot{h}_i, l_m, N) \frac{\partial^2 p_i}{\partial z_i^2} = 12\dot{h}_i \quad (\text{II.5})$$

$$\text{Or:} \quad G(\dot{h}_i, l_m, N) = \frac{h_i}{\mu} [h_i^2 + 12l_m^2 - 6Nl_m h_i \frac{1 + ch(Nh_i / l_m)}{sh(Nh_i / l_m)}] \quad (\text{II.6})$$

$$N = \left( \frac{k_v}{2\mu + k_v} \right)^{1/2}; \mu_v = \mu + \frac{1}{2}k_v; l_m = \left( \frac{\gamma_v}{2\mu} \right)^{1/2} \quad (\text{II.7})$$

$P_i$  is the micropolar pressure field for each pad;  $\mu$  and  $\mu_v$  represent the viscosity coefficient of the Newtonian fluid and the dynamic viscosity coefficient of the micropolar fluid, respectively.

➤ **Boundary Conditions**

To solve the modified Reynolds equation, we assume:

- \_ At the outer boundary, the pressures at the nodes are zero;
- \_ The pressure in the recess is constant and equal to  $P_{ri}$
- \_ To avoid cavitation, negative pressure is set to zero during the iterative calculation process;
- \_ The outgoing flow rate is equal to the incoming flow rate.

**II.2.1.1 Discretization of the Modified Reynolds Equation:**

The discretization of the modified Reynolds equation is done by subdividing the domain into a network of elementary rectangles (mesh). The continuous variables X and Z are replaced by discrete variables I and J.

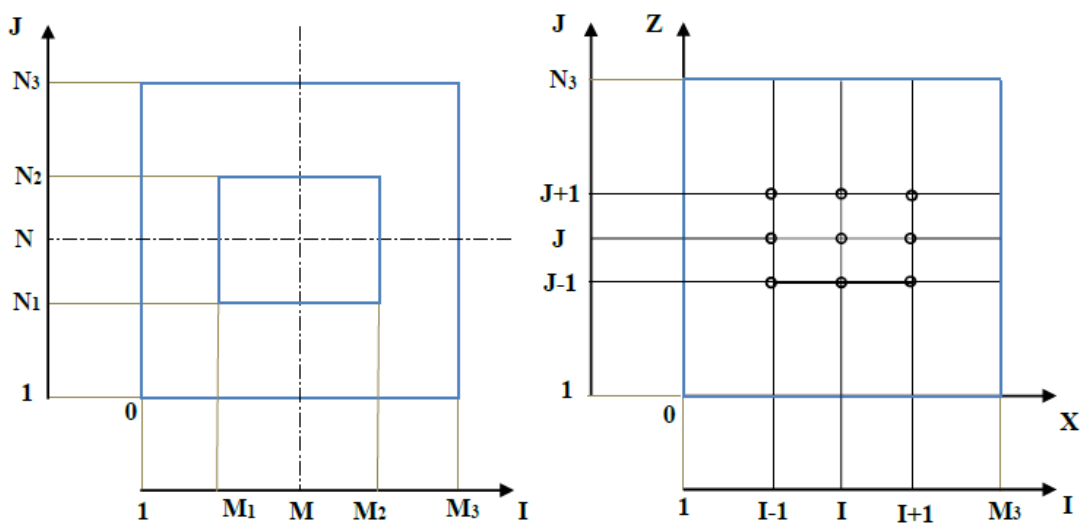


Figure II.4 Calculation domain [29].

The node locations are shown in Figure II.5. Using Taylor's expansion, the value of pressure  $P$  at a point with coordinates  $I$  and  $J$  depends on the pressure values at points neighboring this same point. We obtain the following equations:

$$\frac{\partial P_i(I, J)}{\partial X} = \frac{P_i(I+1, J) - P_i(I-1, J)}{2\Delta X} \quad (\text{II.8})$$

$$\frac{\partial P_i(I, J)}{\partial Z} = \frac{P_i(I, J+1) - P_i(I, J-1)}{2\Delta Z} \quad (\text{II.9})$$

$$\frac{\partial^2 P_i(I, J)}{\partial X^2} = \frac{P_i(I+1, J) - 2P_i(I, J) + P_i(I-1, J)}{2\Delta X^2} \quad (\text{II.10})$$

$$\frac{\partial^2 P_i(I, J)}{\partial Z^2} = \frac{P_i(I, J+1) - 2P_i(I, J) + P_i(I, J-1)}{2\Delta Z^2} \quad (\text{II.11})$$

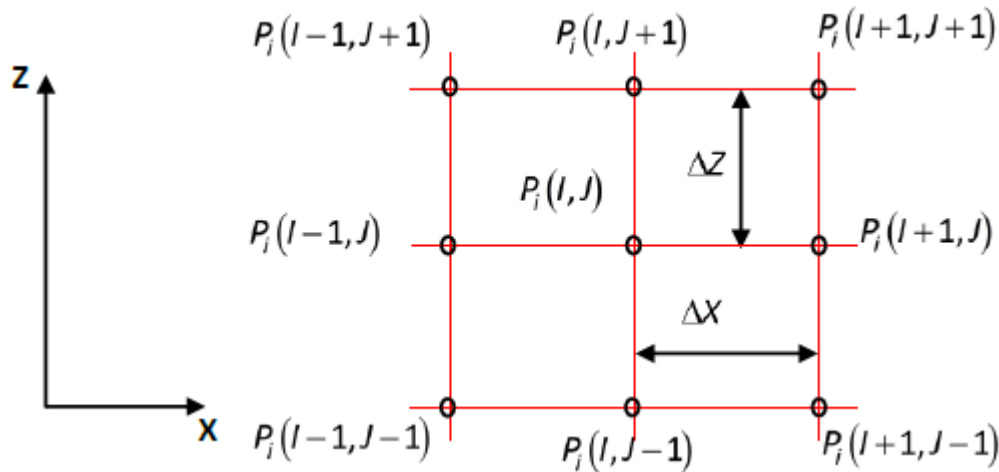


Figure II.5 Description of a node [29].

$\Delta X$  and  $\Delta Z$  represent the steps, i.e., the distances separating two consecutive points along  $X$  and  $Z$  respectively.

By substituting the obtained expressions into the Reynolds equation (II.5), we obtain the following relationship for each node in the integration domain:

$$\frac{12h_i}{G(h_i, l_m, N)} = -2 \left( \frac{1}{\Delta X^2} + \frac{1}{\Delta Z^2} \right) P_i(I, J) + \frac{1}{\Delta X^2} (P_i(I+1, J) - P_i(I-1, J)) + \frac{1}{\Delta Z^2} (P_i(I, J+1) - P_i(I, J-1)) \quad (\text{II.12})$$

### II. 2.1.2 Numerical Solution of the System of Equations:

To solve the system of (M3 N3) equations, we choose the iterative Gauss-Seidel method with an over-relaxation coefficient. To apply this method, it is sufficient to write the finite difference equation in the following form:

$$P_i(I, J)^{(K+1)} = (1-\Omega)P_i(I, J)^K + \Omega \left( CR_i + CJ_i \left( P_i(I+1, J)^{(K+1)} \right) + P_i(I-1, J)^{(K+1)} \right) + CI_i \left( P_i(I, J+1)^{(K+1)} \right) + P_i(I, J-1)^{(K+1)} \quad (\text{II.13})$$

$$CR_i = \frac{12h_i}{G(h_i, l_m, N)} CP, CJ_i = \frac{CP}{\Delta X^2}, CI_i = \frac{CP}{\Delta Z^2}, CP = \frac{\Delta X^2 \times \Delta Z^2}{2(\Delta X^2 + \Delta Z^2)} \quad (\text{II.14})$$

With:  $(1.4 < \Omega < 1.8)$

To reduce the dimensions of the problem, and consequently the time and space required for computation, the symmetry of the integration domain with respect to the X and Z axes is utilized by considering only one-quarter of the study domain (Figure II.6).

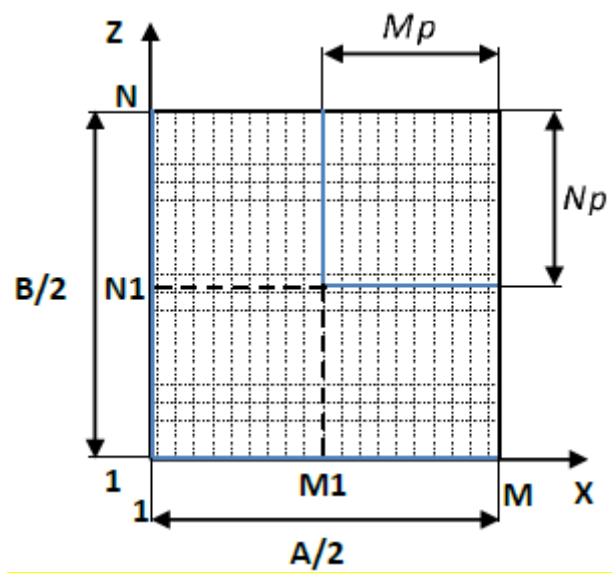


Figure II.6: Discretization of one-quarter of the integration domain [29].

- The steps  $\Delta X$  and  $\Delta Z$  are determined using the following relation:

$$\Delta X = \frac{A}{2CA(MP-1)}, \Delta Z = \frac{B}{2CB(NP-1)} \quad \text{With: } CA = A/a \text{ and } CB = B/b \quad (\text{II.15})$$

- M and N represent the number of mesh cells in the domain along X and Z, respectively, where:

$$M = CA(MP - 1) + 1 \text{ and } N = CB(NP - 1) + 1 \quad (\text{II.16})$$

- MP and NP represent the number of mesh cells in the supply domain (the recess) along X and Z, respectively.

➤ **Boundary Conditions**

To integrate the modified Reynolds equation, it is necessary to consider the pressure in the recess and the boundary conditions of the pressures on the walls:

$$1) \text{ For: } \begin{cases} I = 1 \text{ et } J = 1, N \Rightarrow P_i(I, J) = P_0 \\ J = 1 \text{ et } I = 1, M \Rightarrow P_i(I, J) = P_0 \end{cases}$$

$$2) \text{ For: } \begin{cases} I \geq M1 \\ J \geq N1 \end{cases} \Rightarrow P_i(I, J) = P_0$$

$$3) \text{ For: } \begin{cases} J = N, I \in ]1, M1[ \\ \left. \frac{\partial P_i(I, J)}{\partial x} \right|_N = 0 \end{cases} \Rightarrow P_i(I, J) \text{ is determined by solving the modified Reynolds equation.}$$

$$4) \text{ For: } \begin{cases} I = M, J \in ]1, N1[ \\ \left. \frac{\partial P_i(I, J)}{\partial z} \right|_N = 0 \end{cases} \Rightarrow P_i(I, J) \text{ is determined by solving the modified Reynolds}$$

equation.

## II. 2.2 Performance characteristics:

### II.2.2.1. Load-carrying capacity:

The load-carrying capacity for each hydrostatic thrust bearing is obtained by integrating the pressure field over the bearing surface.

$$W_{pi} = \int_s P_i dS = \int_0^A \int_0^B P_i dx dy \quad (II.17)$$

Here, S is the contact surface and dS is an element of surface.

The load-carrying capacity is determined by integrating the pressure field using the Trapezoidal numerical integration method.

The load-bearing capacity  $W_p$  of the entire set of pads is determined as follows:

$$W_P = \sqrt{W_{Px}^2 + W_{Py}^2} \quad (II.18)$$

While:

$$\begin{cases} W_{Px} = W_{P2} - W_{P4} \\ W_{Py} = W_{P1} - W_{P3} \end{cases} \quad (II.19)$$

### II.2.2.2. Recess pressure:

The recess pressure for each thrust bearing #i is determined by solving the conservation equation for volumetric flow rate:

$$Q_{ri} = Q_{vi} + Q_{si} \quad (II.20)$$

- The flow rate due to the volume change in the recess  $Q_{vi}$  relative to thrust bearing #i is given by:

$$Q_{vi} = S_r \dot{h}_i \quad (II.21)$$

- $Q_{si}$  denotes the volumetric flow rate exiting the recess relative to the single-acting thrust bearing #i (Figure II.7).

## Chapter II: Hydrostatic Bearing with four pads Lubricated by a Micropolar Fluid.

Where: 
$$Q_{si} = Q_{xi}^- + Q_{xi}^+ + Q_{zi}^- + Q_{zi}^+ \quad (\text{II.22})$$

and due to symmetry, the exiting flow rate can be written as follows:

$$Q_{si} = 2(Q_{xi}^- + Q_{zi}^-) \quad (\text{II.23})$$

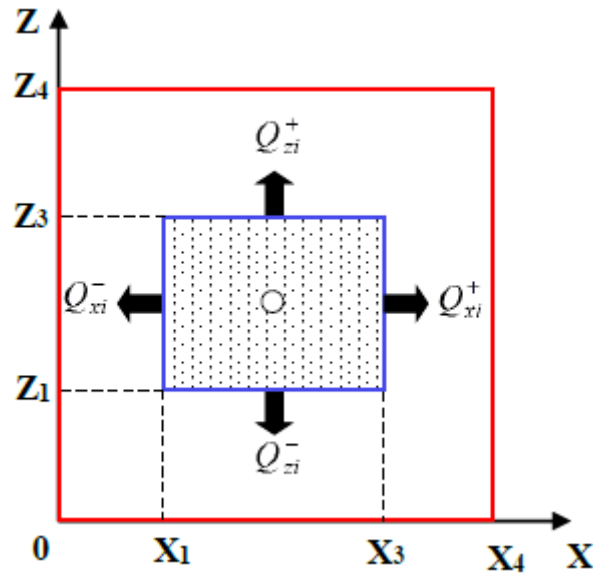


Figure II.7: Flow rate exiting the recess [29].

- The flow rate exiting each thrust bearing in the xi direction is obtained by integrating equation (II.24).

$$Q_{xi}^- = 2 \int_{Z1}^{Z2} \int_0^{h_i} u_{xi} dy_i dz_i \quad (\text{II.24})$$

- The flow rate exiting each thrust bearing in the zi direction is obtained by integrating equation (II.25).

$$Q_{zi}^- = 2 \int_{X1}^{X2} \int_0^{h_i} u_{zi} dy_i dx_i \quad (\text{II.25})$$

## Chapter II: Hydrostatic Bearing with four pads Lubricated by a Micropolar Fluid.

---

The flow rates exiting the recess can be calculated using the Trapezoidal numerical integration method, resulting in one quarter of the integration domain:

$Q_{ri}$  is the flow rate through a capillary-type hydraulic resistance, where:

$$Q_{ri} = \int_0^R 2\pi r u(r) dr \quad (\text{II.26})$$

The flow rate of the micropolar fluid through a capillary-type hydraulic resistance is obtained by integrating equation (II.26):

$$Q_{ri} = \frac{\pi R^4}{8\mu l_c} (P_s - P_{ri}) \varphi(R) \quad (\text{II.27})$$

### II.2.2.3. Total lubricant flow rate:

The total flow rate  $Q_T$  is obtained by summing the flow rates  $Q_{si}$  relative to each thrust bearing, resulting in:

$$Q_T = \sum_{i=1}^4 Q_{si} \quad (\text{II.28})$$

### II.2.2.4. Dynamic characteristics:

A linear study is conducted assuming the shaft is perfectly rigid and limiting to small displacements around a static equilibrium position. To do this, we need to go through two steps:

- A static analysis to determine the equilibrium position of the shaft inside the bearing under an external load;
- A linearized dynamic analysis for the movement of the moving grain (the shaft line) around the static equilibrium position O.

This linear analysis of the behavior of a thrust bearing around the static equilibrium position allows us to model the lubricating film with stiffness and damping coefficients (Figure II.8).

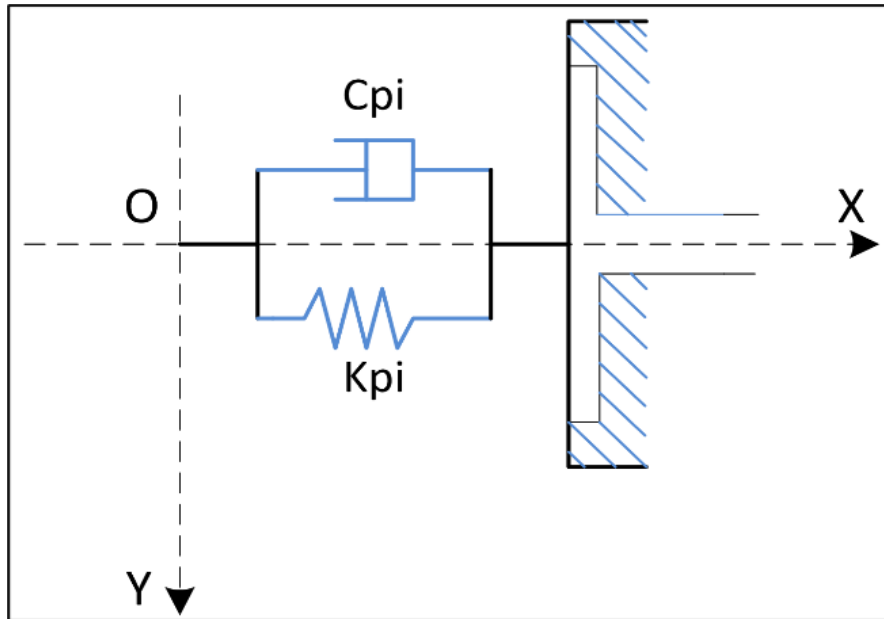


Figure II.8: Stiffness and damping of the  $i$ th hydrostatic bearing pad [29].

The determination of these coefficients allows us to:

- Determine the stability of an operating point (critical mass);
- Introduce the effect of the fluid film on the response of a structure (shaft line subjected to low-amplitude dynamic loads);
- Search for the critical speeds of the shaft line.

**a) Dynamic coefficients of a single-acting hydrostatic thrust bearing**

The calculation of the dynamic coefficients is done using a method known as small displacements and small velocities. If a small displacement  $x_i$  and a small velocity of displacement  $\dot{x}_i$  are imposed near the static equilibrium position  $(x_0, y_0)$ , collinear with the axis  $(o, x)$ , we can write [3]:

$$W_{pi}(x_0 + x_i, y_0, \dot{x}_i, \dot{y}_i = 0) = W_{pi}(x_0, y_0, 0, 0) + x_i \left( \frac{\partial W_{pi}}{\partial x_i} \right)_0 + \dot{x}_i \left( \frac{\partial W_{pi}}{\partial \dot{x}_i} \right)_0 + \dots \quad (II.29)$$

Limiting to the first order, we can write equation (II.29) as follows:

$$W_{pi}(x_0 + x_i, y_0, \dot{x}_i, \dot{y}_i = 0) - W_{pi}(x_0, y_0, 0, 0) = -K_{pi}x_i - C_{pi}\dot{x}_i \quad (II.30)$$

## Chapter II: Hydrostatic Bearing with four pads Lubricated by a Micropolar Fluid.

The coefficients  $K_{pi}$  and  $C_{pi}$  represent the stiffness and damping coefficients due to the presence of the lubricating film in the single-acting hydrostatic thrust bearing #i, near the static equilibrium point. They are obtained after identifying equations (II.29) and (II.30) as follows :

$$K_{pi} = - \left( \frac{\partial W_{pi}}{\partial x_i} \right)_0 \quad (II.31)$$

$$C_{pi} = - \left( \frac{\partial W_{pi}}{\partial \dot{x}_i} \right)_0 \quad (II.32)$$

The stiffness and damping coefficients are calculated using the numerical differentiation method where the partial derivatives are computed numerically.

The application of this method involves the following steps:

- Finding the static equilibrium position characterized by  $(x_0, y_0)$  ;

- Calculating the derivative  $\frac{\partial W_{p1}}{\partial x_1}$  the equation is solved for the position of the center of the moving grain defined by:  $(x_1 = \Delta x_0, y_1 = 0, \dot{x}_1 = 0, \dot{y}_1 = 0, )$  ;

Integrating the pressure field allows us to calculate  $W_{p1}$  at this position, thus:

$$K_{p1} = - \frac{\partial W_{p1}}{\partial x_1} = - \frac{W_{p1}(x_0 + \Delta x_0, y_0, 0, 0) - W_{p1}(x_0, y_0, 0, 0)}{\Delta x_0} \quad (II.33)$$

Calculating the derivative  $\frac{\partial W_{p1}}{\partial \dot{x}_1}$  the equation is solved for each position defined by:

$(x_1 = 0, y_1 = 0, \dot{x}_1 \neq 0, \dot{y}_1 = 0, )$  thus:

$$C_{pi} = - \frac{\partial W_{p1}}{\partial \dot{x}_1} = - \frac{W_{p1}(x_0, y_0, \dot{x}_1, 0) - W_{p1}(x_0, y_0, 0, 0)}{\dot{x}_1} \quad (II.34)$$

**II.2.2.5 Equivalent Dynamic Coefficients:**

The equivalent dynamic characteristics of the bearing are written as follows:

$$K_{epx} = K_{p2} + K_{p4} ; K_{epy} = K_{p1} + K_{p3} \quad (II.35)$$

$$C_{epx} = C_{p2} + C_{p4} ; C_{epy} = C_{p1} + C_{p3} \quad (II.36)$$

Where  $K_{epx}$  and  $K_{epy}$  represent the equivalent stiffness coefficients in the x and y directions, respectively. While  $C_{epx}$  and  $C_{epy}$  represent the equivalent damping coefficients in the x and y directions, respectively.

The damping ratio  $\zeta$  in the x and y directions is expressed as follows:

$$\zeta_x = \frac{C_{epx}}{2\sqrt{MK_{epx}}} ; \zeta_y = \frac{C_{epy}}{2\sqrt{MK_{epy}}} \quad (II.37)$$

**II.3 Validation of the Numerical Model:**

To validate the numerical model proposed in this study, an analytical model is developed for an HSFDF with an incompressible fluid. The HSFDF is assumed to be infinitely long in the OX direction (Figure II.9). The pressure distribution and load-carrying capacity can be obtained from an analytical solution for both Newtonian and micropolar lubricants. Therefore, under the assumptions adopted for a hydrostatic bearing used as a "hydrostatic squeeze film damper" operating with Newtonian or micropolar lubricants, the Reynolds equation (II.5) reduces to:

$$G(\dot{h}_i, l_m, N) \frac{\partial^2 p_i}{\partial z_i^2} = 12\dot{h}_i \quad (II.38)$$

By double integration of equation (2.40) and with the boundary conditions for pressure (as shown in Figure II.9):

$$\begin{cases} p_i = p_{ri} & \text{pour } -b \leq Z \leq 0 \\ p_i = 0 & \text{pour } Z = (B-b)/2 \text{ et } Z = -(B+b)/2 \end{cases} \quad (II.39)$$

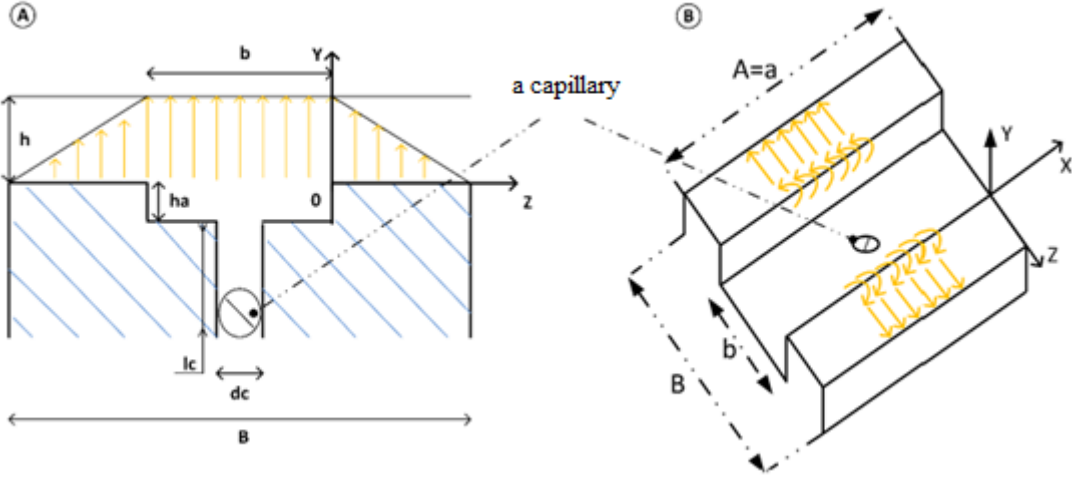


Figure II.9 Pad of the infinitely long hydrostatic thrust bearing [29].

**II.4 Conclusion:**

In this chapter, we have developed a mathematical model to describe the behavior of hydrostatic bearings with four pads lubricated by micropolar fluids. The unique flow characteristics of micropolar fluids, characterized by internal rotational motion of particles, introduce complexities that differ from conventional Newtonian fluids.

Through the formulation of governing equations and numerical methods, we have gained insights into the hydrodynamic performance of the bearing, including pressure distribution, film thickness, and load-carrying capacity. This mathematical framework provides a solid foundation for understanding the dynamic behavior of the bearing and will guide our numerical analysis and optimization efforts in the subsequent chapter.

# **Chapter III:**

## **Results and discussions**

### III.1 Introduction:

In this chapter, we analyze the influence of micropolar fluid parameters on key performance metrics of a four-pad hydrostatic bearing, including pressure distribution, stiffness coefficient, damping coefficient, damping factor, load-carrying capacity, and fluid flow. Through detailed numerical modeling and simulations, we explore how these unique fluid properties affect the bearing's operational efficiency and stability. Our findings offer valuable insights for optimizing the design and functionality of hydrostatic bearings in high-performance rotating machinery, contributing to advancements in lubrication and tribology.

### III.2 Solution procedure:

To determine the pressure field generated on the hydrostatic bearing flat pads, the modified Reynolds Equation [9] is expanded into its finite difference form, and solved by the Gauss Seidel method. The pressure in the recess is determined by solving the flow continuity equation via the secant method, when considering given values for the eccentricity ratio  $\varepsilon$ , the coupling number  $N$ , pressure ratio  $\beta_0$  and the dimensionless characteristic length of the micropolar fluid  $L_m$ . The eccentricity is determined considering that  $e = (\varepsilon * h_0)$ .  $L_m$  is determined based on the relation  $l_m = (h_0 / L_m)$ , where the film thickness  $h_0$  is determined after the solution (secant method) of the flow continuity equation [7]. The convergence tolerances for the pressure, recess pressure and film thickness were set to  $\left( \left( \frac{P_{i,j}^n - P_{i,j}^{n-1}}{100 P_{ri}} \right)_{\max} = 0.01 \right)$ ,  $10^{-6}$  and  $10^{-6}$ , respectively, where  $P_{i,j}^n$  represents the computed pressure at each mesh point (i,j), and  $n$  is the iteration number.

### III.3 Results and discussion:

The analysis described in the present work has been realized after computing the performance characteristics of a four-pad HSFD with respect to the micropolar property for varying pad dimensions and eccentricity ratios. Table 1 shows the numerical parameters considered for the computations.

Parameters	SI
Bearing dimension ratio $A/B$	1
Recess dimension ratio $a/A=b/B$	0.5
capillary diameter $dc$	0.0012 m
capillary length $lc$	0.058 m
viscosity coefficient $\mu$	0.0135 Pa.s
supply pressure $P_s$	50 Bar
Rotor mass $M$	50 Kg

Table III.1 Simulation parameters.

### III.4 Validation of numerical model:

In order to check the validity of the numerical model, an analytical model is developed for an infinitely long hydrostatic bearing pad ( $A/B=6$ ;  $A=a$ ;) lubricated with an incompressible fluid and assumed to be infinitely long in the Ox direction which allows to neglect the lubricant flow in the x direction. Therefore, for bearing operating with Newtonian or micropolar lubricants, the Reynolds Equation [9] reduces to:

$$G(h_i, l_m, N) \frac{\partial^2 p_i}{\partial z_i^2} = 12 \dot{h}_i \quad (III.1)$$

It must be noted that the analytical results presented by computing the stiffness versus the pressure ratio for different values of  $N^2$  and  $L_m$  with  $\varepsilon = 0.2$  using the following equations:

$$h_0 = \left( \frac{(1-\beta_0) K_c}{\beta_0 K_{wf}} \right)^{1/3} \quad (III.2)$$

$$K_{pi} = \frac{20 W_{pi}}{h_0} \left( 1 - \frac{P_{r\dot{h}}}{P_{ri}} \right) \quad (III.3)$$

The recess pressure is determined by solving the following flow continuity equation:

$$Q_{ri} = Q_{vi} + Q_{ozi} \quad (III.4)$$

where

$$P_{r\dot{h}} = 1 / \left( 1 + \frac{K_{wf} \mu G(\dot{h}, l_m, N)}{K_c \varphi(R) + 1} \right) \quad (III.5)$$

$$P_{ri} = 1 / \left( 1 + \frac{K_{wf} \mu G(h_i, l_m, N)}{K_c \varphi(R) + 1} \right) \quad (III.7)$$

$P_{ri}$  is the recess pressure of the  $i^{\text{th}}$  hydrostatic bearing pad;  $P_{r\dot{h}}$  is the recess pressure for ( $h = \dot{h} = h_0 \pm e$ );  $W_{pi}$  is the hydrostatic load relative to each hydrostatic bearing pad ( $W_{pi} = P_{ri} K_{ws} P_s S_p$ );  $K_c$  is the capillary coefficient ( $K_c = \pi d_c^4 / 128 l_c$ );  $K_{wf}$  and  $K_{ws}$  are the first and second load carrying coefficients respectively, ( $K_{wf} = A / 3 b$ ); ( $K_{ws} = (1 + b / B) / 2$ ).

Figure III.1 compares the numerical prediction of the equivalent stiffness obtained for various values of  $N^2$  and  $L_m$  with the analytical results, and demonstrates a close correspondence between the evaluations. The comparison was conducted while employing the following parameters  $P_s = 50$  Bar,  $\mu = 0.0135$  Pa.s, ( $A/B=6$ ;  $A=a$ ). It should be noted that the equivalent stiffness has an optimum value obtained for a pressure ratio equal to 0.65 in the case of Newtonian lubricant (Fig.3 (a)), while in case of micropolar lubricant and for any values of  $N^2$  and  $L_m$  the optimum one is obtained for  $0.45 \leq \beta_0 \leq 0.6$  where for  $N^2 = 0.3$ ;  $L_m = 5$  (Figure III.1 (b)), the optimum value is obtained for  $\beta_0 = 0.6$ , while for  $N^2 = 0.7$ ;  $L_m = 5$  (Figure III.1 (c)), the optimum one is obtained for  $\beta_0 = 0.45$  and in the case of  $N^2 = 0.7$ ;  $L_m = 10$  (Figure III.1 (d)), the equivalent stiffness has an optimum value obtained for  $\beta_0 = 0.55$ . In fact, the maximum deviation observed in the graphs of Figure III.1 is less than 0.95% for micropolar lubricant (Figure III.1 (d)) at  $\beta_0 = 0.5$  while for Newtonian lubricant is

about 0.87% at  $\beta_0 = 0.7$ . A minimum deviation of about 0.34% and 0.40% are noted for Newtonian and micropolar lubricant (Figure III.1 (c)), respectively, at minimum pressure ratio values. The numerical procedure is therefore considered offering a high level of precision for both Newtonian and micropolar lubricants. Consequently, the comparisons confirm the validity of the numerical model.

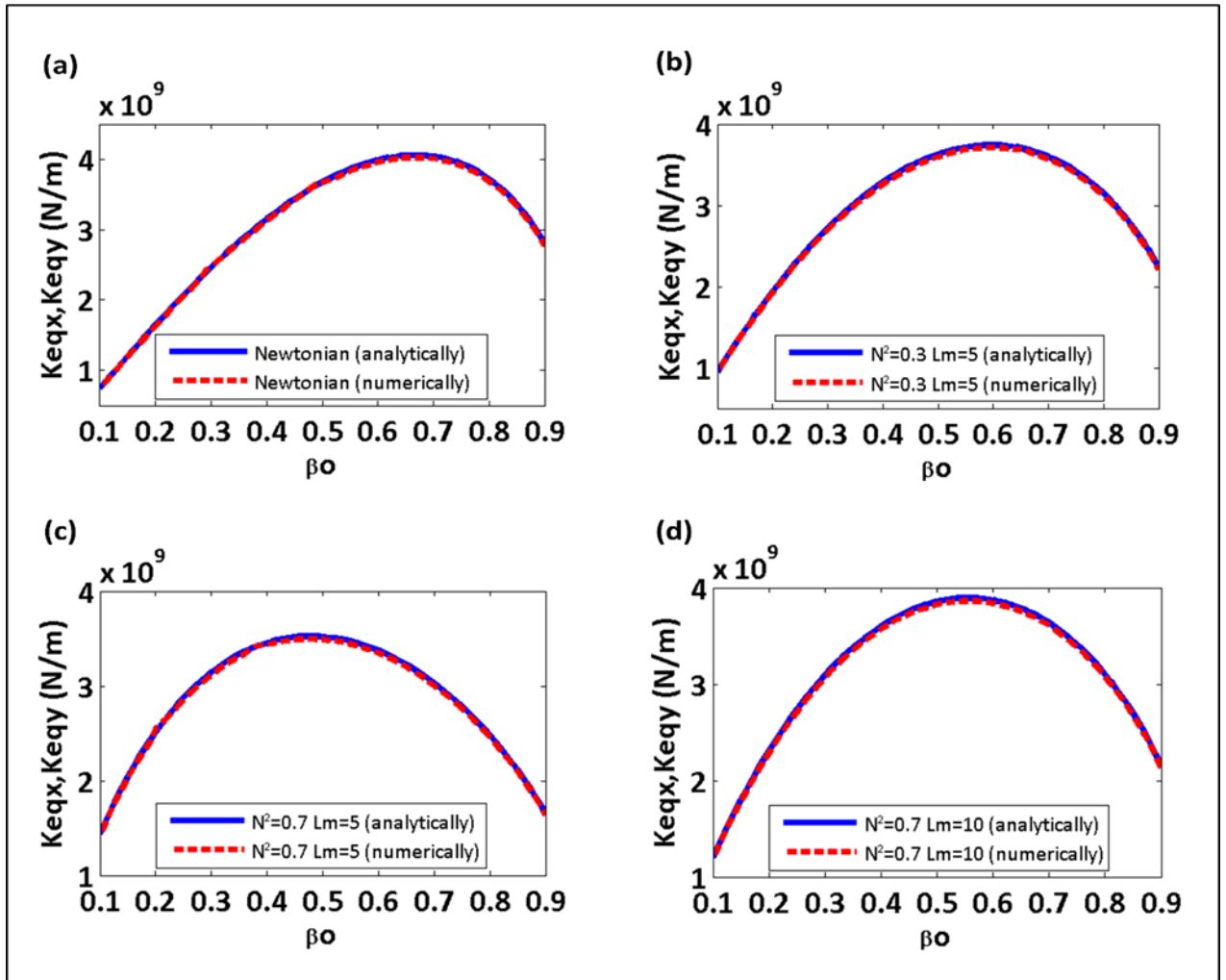


Figure III.1 Comparison of the numerical and analytical results: variation of the equivalent stiffness with pressure ratio for various values of  $N^2$  and  $L_m$  ( $A/B = 6$ )

### III. 5 Study of the influence of micropolar fluid parameters:

#### III.5.1 Influence of micropolar fluid parameters on pressure profile:

The variations of the pressure distribution for various values of  $N^2$  with  $L_m = 5$  and  $\varepsilon = 0.2$  are presented in Figure III.2. These plots show that the pressure distribution covers the entire bearing pad area, does not demonstrate any pressure concentration, and decreases following a linear variation for all the various values of  $N^2$ . It is found that the coupling number increases the pressure inside the recess at lower values of  $L_m$ .

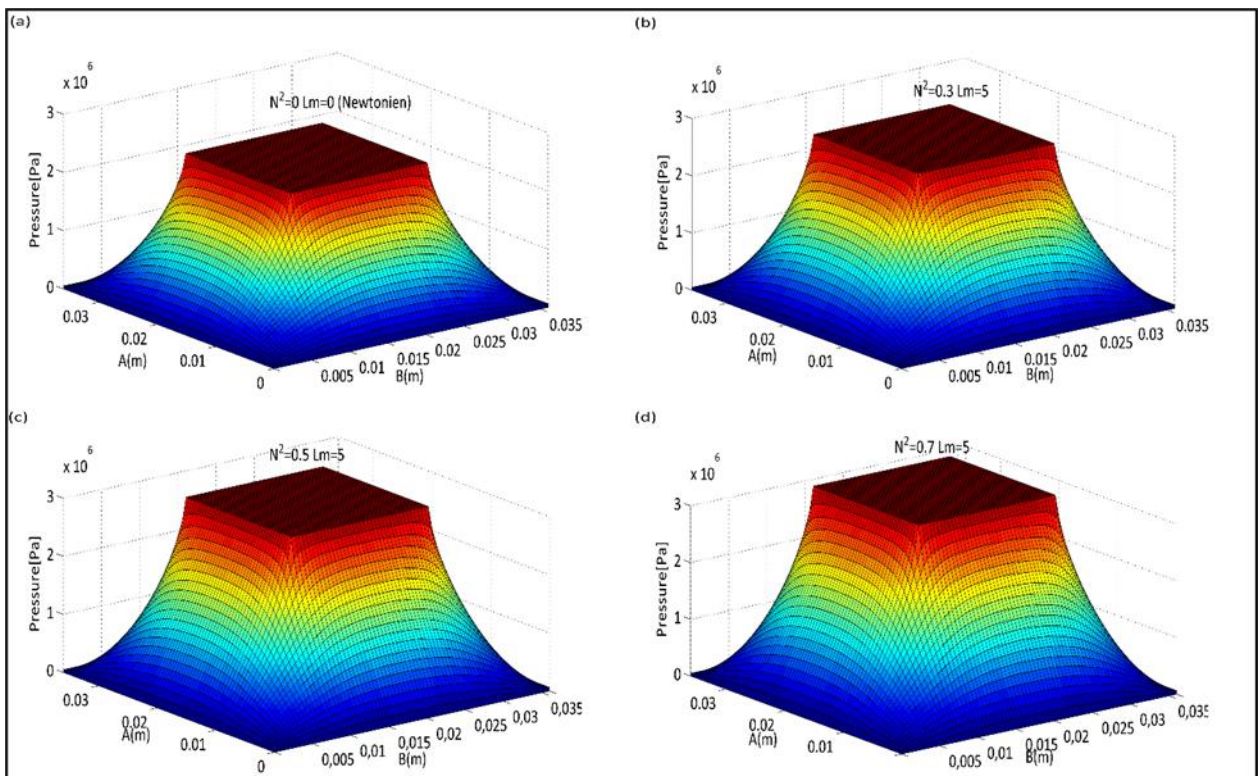


Figure III.2: Pressure distribution for various values of  $N^2$  with  $L_m = 5$

#### III.5.2 Influence of micropolar fluid parameters on equivalent stiffness:

Figure III.3 shows the variation of the equivalent stiffness for different values of  $N^2$ . These curves indicate that when compared to the Newtonian lubricant the value of the micropolar lubricant equivalent stiffness is higher for  $\varepsilon < 0.4$  while, when  $\varepsilon > 0.4$ , the equivalent stiffness of the Newtonian lubricant is higher. The equivalent stiffness also rapidly increases with  $\varepsilon$ .

Figure III.4 presents the equivalent stiffness variations with  $L_m$  for different values of the bearing dimension ratio and  $N^2 = 0.5$ . This figure shows that for bearings operating with

micropolar lubricants, there is an optimal value for bearing dimension ratio producing the maximum value of the equivalent stiffness. Moreover, the curves in Figure III.4 show that for  $L_m > 10$ ,  $K_{eq}$  decreases with an increase in  $L_m$ .

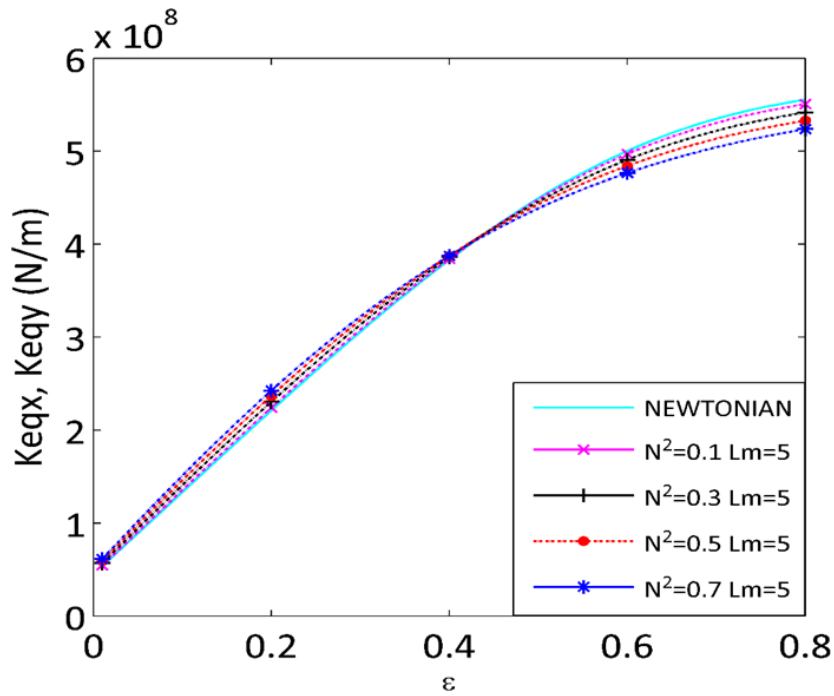


Figure III.3: Variation of equivalent stiffness as a function of eccentricity ratio for various values of  $N^2$  with  $L_m=5$

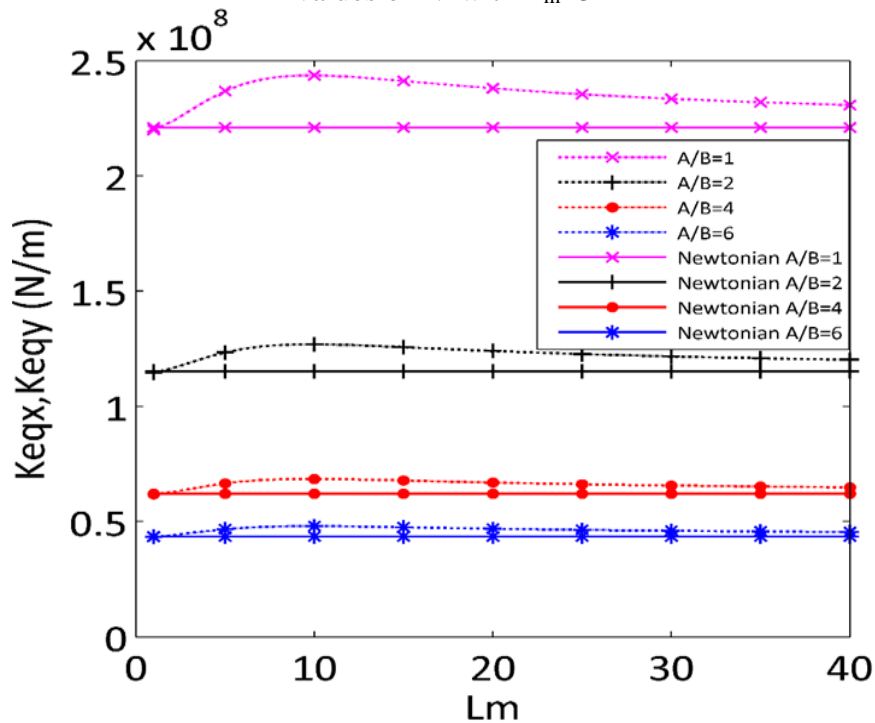


Figure III.4: Variation of equivalent stiffness as a function of  $L_m$  for various values of bearing dimension ratio with  $N^2=0.5$

### III.5.3 Influence on equivalent damping:

Figure III.5 presents the variation of the equivalent damping with the eccentricity ratio and various values of the coupling number  $N^2$ . The presented results reveal that the equivalent damping increases with  $\varepsilon$  augmentations, and rises with  $N^2$  increases. The physical reason explaining the above observation is that an increase in  $N^2$  means stronger coupling effects between the angular and linear momentum. This coupling effect leads to enhanced effective viscosity, and therefore to equivalent damping augmentations.

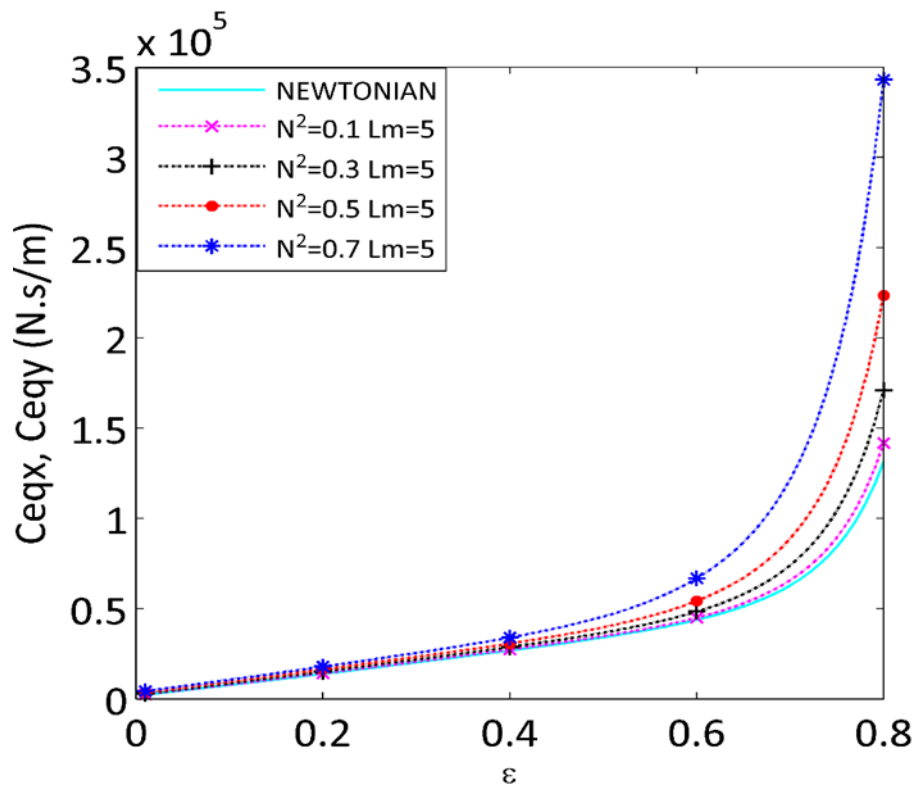


Figure III.5: Variation of equivalent damping as a function of eccentricity ratio for various values of  $N^2$  with  $L_m=5$

Figure III.6 plots the equivalent damping against  $L_m$  for different values of bearing dimension ratio and  $N^2 = 0.5$ . This figure shows that bearing dimension ratio ( $A/B=1$ ) provide larger value of the equivalent damping with both micropolar and Newtonian lubricants. This response of the equivalent damping results from pressure increases inside the recesses also associated with film thickness reductions. The equivalent damping also increases with an  $L_m$  reduction, particularly below 5.

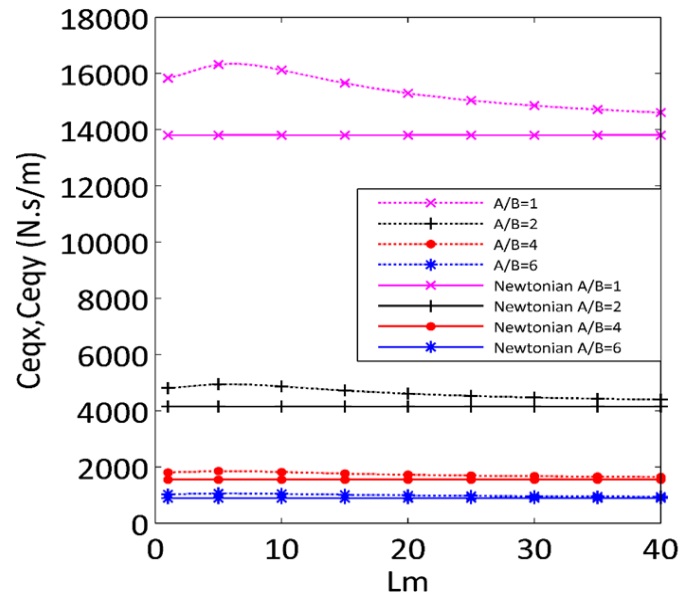


Figure III.6: Variation of equivalent damping as a function of  $L_m$  for various values of bearing dimension ratio with  $N^2=0.5$

### III.5.4 Influence on damping factor:

The effect of eccentricity ratio on the damping factor is displayed in Figure III.7 for variations of  $N^2$  when  $L_m$  remains fixed at 5. The presented results indicate that regardless of  $N^2$ , the damping factor increases with  $\varepsilon$ . Moreover, the maximum damping factor value increases with  $N^2$ . This increase results from a pressure augmentation inside the recess associated with low  $L_m$  value.

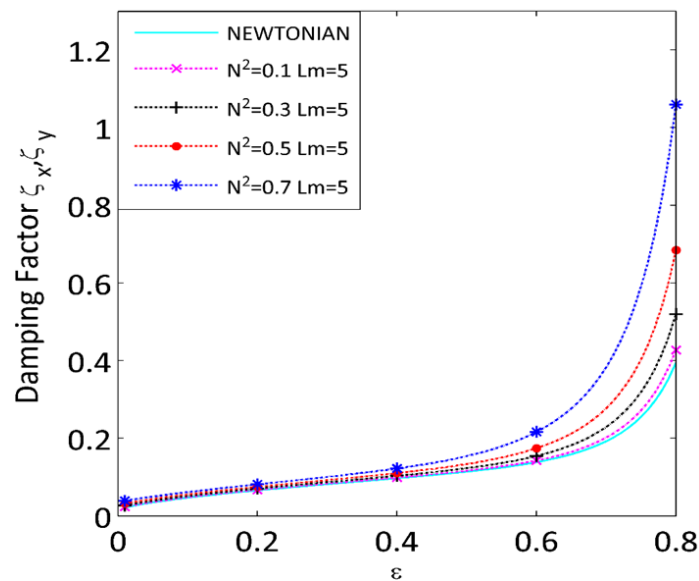


Figure III.7: Variation of damping factor as a function of eccentricity ratio for various values of  $N^2$  with  $L_m=5$

Figure III.8 presents the damping factor variations with the dimensionless characteristic length parameter  $L_m$  for different values of bearing dimension ratio and  $N^2 = 0.5$ . It is observed that damping factor decreases accordingly with bearing dimension ratio, while the micropolar fluid response reduces to a Newtonian one as  $L_m$  grows. The graph of Figure III.8 also suggests that there is an optimum value of  $L_m$  at which the damping factor of each bearing dimension ratio is maximum. This maximum also raises with increase in bearing dimension ratio.

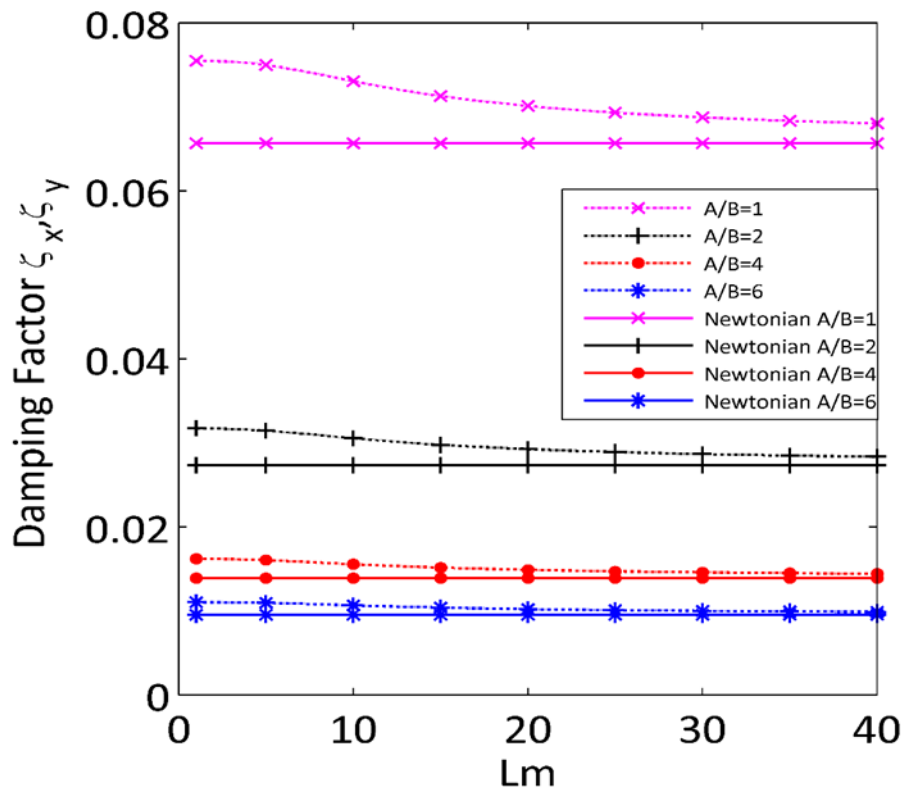


Figure III.8 Variation of damping factor as a function of  $L_m$  for various values of bearing dimension ratio with  $N^2 = 5$

### III.6 Conclusion:

This chapter has shown that micropolar fluid parameters significantly impact the performance of four-pad hydrostatic bearings. Our numerical analysis highlighted effects on pressure distribution, stiffness, damping, load-carrying capacity, and fluid flow. These findings demonstrate the potential of micropolar fluids to enhance bearing performance, offering improved stability and reduced friction. This research lays the groundwork for further advancements in the design and optimization of hydrostatic bearings in high-performance machinery.

# **General conclusion**

### General conclusion

In conclusion, our numerical study on the dynamic behavior of a four-pad hydrostatic bearing lubricated by a micropolar fluid has provided valuable insights for the design and optimization of mechanical systems. Advanced numerical modeling and finite element simulations have illuminated the complex interactions between bearing components, micropolar fluid, and operating conditions. This research highlights the significant impact of micropolar fluids' rheological properties on hydrostatic bearings, particularly in reducing friction, enhancing dynamic stability, and optimizing performance metrics such as pressure distribution, stiffness, damping, and load-carrying capacity.

Key findings include the observation that micropolar fluids improve tribological performance compared to Newtonian fluids, notably through increased pressure in recesses and enhanced damping and stiffness for specific bearing dimension ratios. Additionally, the coupling number and eccentricity ratio significantly influence fluid flow rates and load-carrying capacities, with micropolar lubricants providing advantages in reducing flow rates and increasing load support under lower bearing dimension ratios.

Our results underscore the importance of fundamental research in lubrication and tribology to address industrial challenges and suggest that incorporating micropolar fluid parameters can lead to more efficient, reliable, and durable mechanical systems. We hope this thesis serves as a foundation for future research and innovation in fluid mechanics, lubrication, and mechanical system dynamics, driving advancements in mechanical engineering and technology development to meet modern industry needs.

# References

## References

- [1] Abed. A "Etude du comportement statique et dynamique de paliers fluides à patins hydrostatiques intelligents", Thèse de Doctorat, UNHB Chlef, Algérie ,2017.
- [2] Delamare, J., & Faure, F. (1998). Les paliers magnétiques. *Revue 3EI*, 2-9.
- [3] Zerrouni, N. (2009). Etude de l'interaction fluide visqueux-structure d'un palier fluide.
- [4] Sahli Abdelkader. Etude Expérimentale D'un Palier Lubrifié Mesaligne, thèse de Magister : Université de Hassiba Ben Bouali-Chlef; 2011
- [5] Hydrostatic bearings – About Tribology. (2024). récupéré April 7, 2024, depuis [www.tribonet.org/wiki/hydrostatic-bearings/](http://www.tribonet.org/wiki/hydrostatic-bearings/)
- [6] Bassani, R., & Piccigallo, B. (1992). *Hydrostatic lubrication* (Vol. 22). Elsevier.
- [7] Zerrouni Nassim. Etude de l'interaction fluide visqueux-structure d'un palier fluide soumis à des sollicitations temporelles, thèse de Magister : Université de M'hamed Bougara-Boumerdes; 2009.
- [8] Belgacem Souad, "Etude du comportement vibratoire non-linéaire d'une ligne d'arbre montée sur paliers hydrostatiques lubrifiés par nanofluides", thèse de doctorat, Université Ibn-khaldoun de Tiaret ,2019.
- [9] Bouzidane, A. (2007). Conception d'un palier hydrostatique intelligent pour contrôler les vibrations de rotors (Doctoral dissertation, École de technologie supérieure).
- [10] Grzegorz Łukaszewicz. *Micropolar Fluids: Theory and Applications*, Springer Science+Business Media, LLC; 1999.
- [11] A.C.ERINGEN, Theory of micropolar fluids, *J. Math. Mech.* 16, No.1 (1966),1-16.
- [12] ERINGEN AC. Simple microfluids. *International Journal of Engineering Science.* 1964;2:205-17.
- [13] Prakash J, Sinha P. Lubrication theory for micropolar fluids and its application to a journal bearing. *International Journal of Engineering Science.* 1975;13:217-32.
- [14] Zaheeruddin K, Isa M. Micropolar fluid lubrication of one-dimensional journal bearings. *Wear.* 1978;50:211-20.
- [15] Tipei N. Lubrication with micropolar liquids and its application to short bearings. *Journal of tribology.* 1979;101:356-63.
- [16] Singh C, Sinha P. The three-dimensional Reynolds equation for micro-polar-fluidlubricated bearings. *Wear.* 1982, 76,199-209.
- [17] Gay Bayada, Nadia Benhaboucha, *Mathematical models and methods in Applied Sciences* 15(03), 343-374, 2005.

- [18] Martin G. Étude numérique des équations d'un fluide micropolaire 2001
- [19] Nicodemus ER, Sharma SC. Orifice compensated multirecess hydrostatic/hybrid journal bearing system of various geometric shapes of recess operating with micropolar lubricant. *Tribology International*. 2011;44:284-96.
- [20] Sharma SC, Ram N. Influence of micropolar lubricants on the performance of slotentry hybrid journal bearing. *Tribology International*. 2011;44:1852-6.
- [21] Dynamique des rotors, sur site *MSC Software*. Consulté le 16/06/2019. <https://www.mssoftware.com/fr/application/dynamique-de-rotors>
- [22] Beyond magnetic bearings, plenty of innovation is taking place in air bearings as well as traditional products get your bearings straight, sur site *turbomachinerymag*. Consulté le 20/06/2019. <https://www.turbomachinerymag.com/get-your-bearings-straight/>
- [23] Boutaleb A, Ben Aissa M. Modélisation et analyse du comportement dynamique d'une ligne d'arbre flexible en régime transitoire, thèse de master : Université Ibn-Khaldoun-Tiaret ; 2015-2016.
- [24] Benariba A, Bouzidane A et Thomas M. Analytical analysis of a rigid rotor mounted on three hydrostatic pads lubricated with micropolar fluids, *Proc IMechE, Part J: Journal of Engineering Tribology*, 2018; 233: 859-869.
- [25] <https://www.btscpi.fr/articles.php?lng=fr&pg=771&mnuid=27032&tconfig=0>
- [26] <http://www.directindustry.fr/prod/zollern/product-13709-777041.html>
- [27] <http://www.directindustry.fr/prod/dresser-rand/paliers-magnetiques-139981160495.html>
- [28] Hydrostatic journal bearings, sur le site rotorlab tamu. Consulté le 20/05/2020. [https://rotorlab.tamu.edu/me626/Notes\\_pdf/Notes12b%20Hydrostatic%20Bearings.pdf](https://rotorlab.tamu.edu/me626/Notes_pdf/Notes12b%20Hydrostatic%20Bearings.pdf)
- [29] Aboubakeur. Contribution à l'étude de la lubrification micropolaire : Applications aux paliers hydrostatiques, thèse de Doctorat : Université Ibn-Khaldoun-Tiaret; 2017-2018.
- [30] <http://www.zoneindustrie.com/Produit/Palier-SE-17641.html>.